AD-A150 010 THIN FILM TECHNOLOGY OF HIGH-CRITICAL-TEMPERATURE SUPERCONDUCTING ELECTRO..(U) WESTINGHOUSE RESEARCH AND DEVELOPMENT CENTER PITTSBURGH PA J TALVACCHIO ET AL. 1/1

UNCLASSIFIED 01 DEC 84 84-9C9-TUDEV-R1 N00014-82-C-0617 F/G 9/3 NL

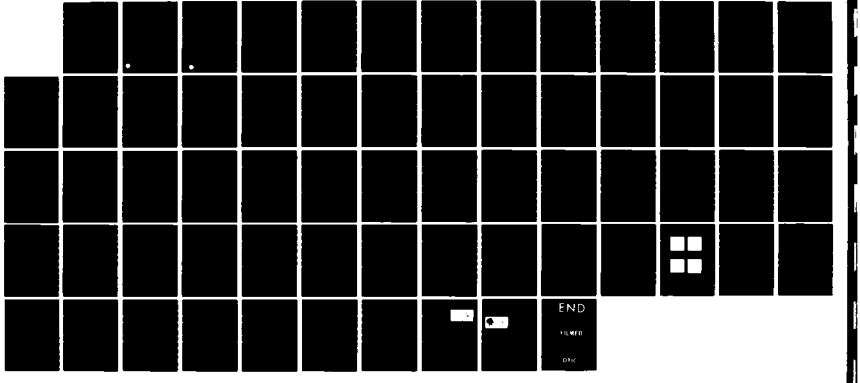

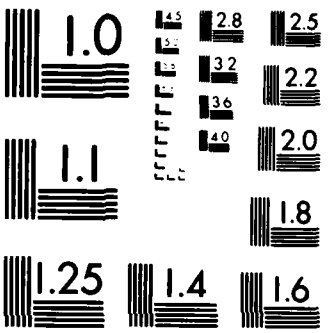

# THIN FILM TECHNOLOGY OF HIGH-CRITICAL-TEMPERATURE SUPERCONDUCTING ELECTRONICS

Annual Report

November 1, 1983 to October 31, 1984

by

J. Talvacchio, A. I. Braginski, and M. A. Janocko

Westinghouse Electric Corporation
Research and Development Center
Pittsburgh, Pennsylvania 15235

ONR Contract No. N00014-82-C-0617



Westinghouse R&D Center
1310 Beulah Road
Pittsburgh, Pennsylvania 15235

# THIN FILM TECHNOLOGY OF HIGH-CRITICAL-TEMPERATURE SUPERCONDUCTING ELECTRONICS

Annual Report

November 1, 1983 to October 31, 1984

by

J. Talvacchio, A. I. Braginski, and M. A. Janocko

Westinghouse Electric Corporation
Research and Development Center
Pittsburgh, Pennsylvania 15235

ONR Contract No. N00014-82-C-0617

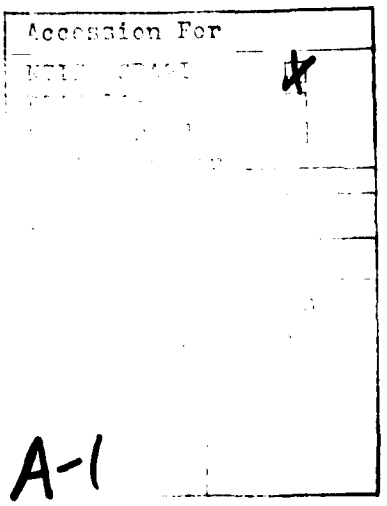


**Westinghouse R&D Center**
**1310 Beulah Road**
**Pittsburgh, Pennsylvania 15235**

Unclassified

SECURITY CLASSIFICATION OF THIS PAGE

## REPORT DOCUMENTATION PAGE

| | |
|---|---|
| 1a. REPORT SECURITY CLASSIFICATION | 1b. RESTRICTIVE MARKINGS |
| 2a. SECURITY CLASSIFICATION AUTHORITY | 3. DISTRIBUTION/AVAILABILITY OF REPORT |
| 2b. DECLASSIFICATION/DOWNGRADING SCHEDULE | |
| 4. PERFORMING ORGANIZATION REPORT NUMBER(S)<br>84-9C9-TUDEV-R1 | 5. MONITORING ORGANIZATION REPORT NUMBER(S) |
| 6a. NAME OF PERFORMING ORGANIZATION<br>Westinghouse Research and Development Center<br>6b. OFFICE SYMBOL (If applicable) | 7a. NAME OF MONITORING ORGANIZATION<br>DCASMA Pittsburgh |
| 6c. ADDRESS (City, State and ZIP Code)<br>1310 Beulah Road<br>Pittsburgh, Pennsylvania 15235 | 7b. ADDRESS (City, State and ZIP Code)<br>1626-S Federal Building<br>1000 Liberty Avenue<br>Pittsburgh, PA 15222 |
| 8a. NAME OF FUNDING/SPONSORING ORGANIZATION<br>Office of Naval Research<br>8b. OFFICE SYMBOL (If applicable) | 9. PROCUREMENT INSTRUMENT IDENTIFICATION NUMBER |
| 8c. ADDRESS (City, State and ZIP Code) | 10. SOURCE OF FUNDING NOS<br>PROGRAM ELEMENT NO. / PROJECT NO. / TASK NO. / WORK UNIT NO. |

11. TITLE (Include Security Classification)
THIN FILM TECHNOLOGY OF HIGH-CRITICAL-TEMPERATURE SUPERCONDUCTING ELECTRONICS

12. PERSONAL AUTHOR(S)
Talvacchio, J., Braginski, A. I., Janocko, M. A.

| 13a. TYPE OF REPORT | 13b. TIME COVERED | 14. DATE OF REPORT (Yr., Mo., Day) | 15. PAGE COUNT |
|---|---|---|---|
| Annual | FROM 11-1-83 TO 10-30-84 | 841201 | 56 |

16. SUPPLEMENTARY NOTATION

| 17. COSATI CODES | | |
|---|---|---|
| FIELD | GROUP | SUB GR |
| | | |
| | | |

18. SUBJECT TERMS (Continue on reverse if necessary and identify by block number)
superconductors, films, Josephson, junctions, niobium, molybdenum, A15, XPS,

19. ABSTRACT (Continue on reverse if necessary and identify by block number)

During the second year of performance under this program, the atomic segregation on A15 surfaces was evaluated and resulted in $Nb_3Sn$ replacing $V_3Si$ as the tunnel junction high-$T_c$ base electrode. A process of all-refractory test junction patterning by wet and/or reactive ion etching was implemented. Epitaxial, textured tunnel barrier structures of the form $Al/Al_2O_3$, $Y/Y_2O_3$, and $Al/Al_2O_3/Al$, have been fabricated. Tunnel junctions with Nbm $Nb_3Sn$, and Mo-Re base and Pb-Bi counterelectrodes have been formed with the barrier structures and had excellent I-V characteristics. Junctions with Nb counterelectrodes exhibited high subgap leakage currents. The $Mo_{65}Re_{35}$ alloy was found to be an ideal material for counterelectrodes having $T_c$ = 12K.

| | |
|---|---|
| 20. DISTRIBUTION/AVAILABILITY OF ABSTRACT<br>UNCLASSIFIED/UNLIMITED ☐ SAME AS RPT ☐ OTIC USERS ☐ | 21. ABSTRACT SECURITY CLASSIFICATION |
| 22a. NAME OF RESPONSIBLE INDIVIDUAL | 22b. TELEPHONE NUMBER (Include Area Code) / 22c. OFFICE SYMBOL |

DD FORM 1473, 83 APR EDITION OF 1 JAN 73 IS OBSOLETE

Unclassified

SECURITY CLASSIFICATION OF THIS PAGE

## TABLE OF CONTENTS


| | Page |
|---|---|
| ABSTRACT | iii |
| LIST OF FIGURES | v |
| 1. INTRODUCTION | 1 |
| 1.1 Program Objective | 1 |
| 1.2 Approach | 2 |
| 1.3 Summary of Results | 3 |
| 2. EXPERIMENTAL APPARATUS AND METHODS | 5 |
| 2.1 Film Deposition | 5 |
| 2.2 Analytical Methods | 8 |
| 2.3 Junction Fabrication from Trilayers Formed *in situ* | 9 |
| 3. RESULTS AND DISCUSSION | 12 |
| 3.1 Task 1 - Superconductor/Barrier Interfaces | 12 |
| 3.2 Task 2 - Analogue to SNAP Process | 23 |
| 3.3 Task 3 - Reference Junctions | 25 |
| 3.4 Task 4 - High-$T_c$ Counterelectrode Fabrication | 40 |
| 3.5 Task 5 - Fabricate and Test High-$T_{op}$ Junctions | 47 |
| 4. CONCLUSIONS | 49 |
| 5. ACKNOWLEDGEMENTS | 50 |
| 6. REFERENCES | 51 |
| APPENDIX "Tunneling and Interface Structure of Oxidized Metal Barriers on A15 Superconductors," Proc. of the 1984 Applied Superconductivity Conference, San Diego, to be published in IEEE Transactions on Magnetics | 53 |

## ABSTRACT

During the second year of performance under this program, the atomic segregation on A15 surfaces was evaluated and resulted in $Nb_3Sn$ replacing $V_3Si$ as the tunnel junction high-$T_c$ base electrode. A process of all-refractory test junction patterning by wet and/or reactive ion etching was implemented. Epitaxial, textured tunnel barrier structures of the form $Al/Al_2O_3$, $Y/Y_2O_3$, and $Al/Al_2O_3/Al$, have been fabricated. Tunnel junctions with Nb, $Nb_3Sn$, and Mo-Re base and Pb-Bi counterelectrodes have been formed with the barrier structures and had excellent I-V characteristics. Junctions with Nb counterelectrodes exhibited high subgap leakage currents. The $Mo_{65}Re_{35}$ alloy was found to be an ideal material for counterelectrodes having $T_c$ = 12K.

## LIST OF FIGURES


Figure 2.1 Schematic of the current status of the SDAF.

2.2 Processing steps to form a tunnel junction from a trilayer formed *in situ*.

3.1 The thicknesses of oxidized aluminum and yttrium overlayers deposited on Nb compared with the nominal thicknesses based on deposition rates. The dashed line indicates agreement between the measured thickness and the nominal value.

3.2 The thicknesses of oxidized aluminum and yttrium overlayers deposited on $V_3Si$ compared with the nominal thicknesses based on deposition rates.

3.3 The normalized thicknesses of three overlayers determined by XPS at a series of detection angles compared with the apparent thickness of an overlayer modeled as having a Gaussian distribution of thickness and $\sigma = 1.0$.

3.4 The apparent thickness of an overlayer with a uniform thickness of 1.0 which is on a rough surface. The substrate is modeled as a sinusoid with a roughness parameter defined as the ratio of the amplitude to the period of the sinusoid.

3.5 The quasiparticle I-V characteristics of four Nb/oxidized Al/Pb-Bi tunnel junctions with barriers of different morphologies. a) Highly-textured evaporated Al b) Amorphous barrier after ion-milling c) Highly-textured sputtered Al d) Randomly-oriented fine-grained Al grown on sputtered polycrystalline Nb.

3.6 The quasiparticle I-V characteristics of two $Nb_3Sn$-based junctions. a) Evaporated (oxidized) Al barrier b) Evaporated (oxidized) Y barrier.

3.7 The I-V curve of a junction with a 200 A thick $Mo_{.65}Re_{.35}$ base electrode, an oxidized Al barrier, and a Pb-Bi counterelectrode.

3.8 An I-V curve typical of all-Nb tunnel junctions.

3.9 The I-V characteristic of a Nb-Sn junction with a Nb counterelectrode.

3.10 Resistive transition temperature plotted as a function of composition for Mo-Re alloys. The dotted line is a fit to data from the bulk samples of reference 15.

3.11 Resistive transition temperature for $Mo_{65}Re_{35}$ alloys plotted as a function of film thickness. The data for the films evaporated on substrates held at 100°C are connected by a solid line. The data for films sputtered at 800°C are connected by a dashed line.

3.12 The resistivity ratio of $Mo_{65}Re_{35}$ alloys plotted as a function of film thickness. The data for the evaporated films are connected by a solid line. The data for films sputtered at 800°C are connected by a dashed line.

3.13 RHEED patterns for four films.

## LIST OF TABLES

Table 3.1 Surface segregation of A15 compounds.

3.2 Summary of junction configurations.

# 1. INTRODUCTION

## 1.1 Program Objective

The overall objective of this program is to develop a technology of thin-film Josephson tunnel junctions capable of operating at temperatures, $T_{op}$ > 10K, compatible with the performance of small closed-cycle refrigerators. This will permit the incorporation of superconducting electronics into electronic warfare and advanced radar systems.

The specific program objective (Phase I) is to demonstrate the technical feasibility of thin film tunnel junctions fabricated from A15 compounds and hard alloy superconductors, such as Mo-Re, having critical temperatures, $T_c$, sufficiently high to achieve useful device characteristics at temperatures exceeding 10K. This will permit a comparison with high $T_c$, B1 structure NbN junctions developed by the Naval Research Laboratory and other R&D organizations in the United States and overseas.

The second year's tasks defined by the Statement of Work are:

Task 2. Develop a selective anodization process for A15 and Mo-Re films.

Task 3. Fabricate and characterize A15 and Mo-Re reference tunnel junctions with low-$T_c$ soft alloy and Nb counterelectrodes.

Task 4. Determine the preferred approach to high-$T_c$ counterelectrode fabrication.

Task 5. (Third year task) Fabricate and test high-operating-temperature (>10 K) prototype tunnel junctions.

## 1.2 Approach

The approach, as outlined in the program proposal and first year's annual report,[1] has changed only in becoming better-defined. It is based on the use of a novel ultra-high-vacuum closed system referred to as the Westinghouse Superlattice Deposition and Analysis Facility (SDAF). This has made possible the *in situ* formation, processing, and characterization (without breaking the vacuum) of multilayered, complete junction structures. These structures have been subsequently patterned into junctions by a process described in section 2.3 of this report.

The approach to formation of a tunnelling barrier has been to deposit a thin (20 to 60 A) metal which forms a mechanically and thermally stable oxide, without suboxides, upon exposure to oxygen. The wetting properties of one metal on another are likely to result in a more complete and uniform coverage than if the oxide was deposited directly. The choice of an oxide barrier was made because some oxides are stable, at least in their bulk form, at the high temperature which may be needed to form a high-$T_c$ counterelectrode.

The key problems to be solved are:

1. To find an artificial tunnelling barrier material that performs well with high-$T_c$ electrodes. This requires that there is no chemical interaction with the electrodes, no diffusion into the electrodes at whatever processing temperature is required, and perhaps a compatibility with the crystalline

structure of the counterelectrode.

2. To form a counterelectrode having a high $T_c$ within a coherence length of the barrier/counterelectrode interface (on the order of 50 A in high-$T_c$ materials). For the A15 materials, this requires a high degree of order in the initial deposit. A choice was made to concentrate on crystalline, epitaxial barriers which have been made possible by the UHV enviroment of the SDAF. The rationale was to create a substrate for counterelectrode deposition that would promote the formation of a crystalline, ordered superconductor.

Mo-Re represents a possible solution to both problems. We have demonstrated that it can be formed at a substrate temperature near room temperature so the barrier does not have to withstand a high processing temperature. It will not oxidize readily even when a fresh surface is exposed to the atmosphere so it will not reduce the barrier. It is relatively insensitive to disorder so the second problem is minimized. However, with a $T_c$ of only 12K, Mo-Re counterelectrodes would be only an intermediate solution.

### 1.3 Summary of Results

During the second year of performance the following major results were obtained:

(a) The investigation of the surface atomic segregation in A15 compounds using X-ray Photoelectron Spectroscopy (XPS) has shown that this effect was most significant in $V_3Si$. Consequently, this material was replaced by $Nb_3Sn$ for use as a

high-$T_c$ base electrode.

(b) A simple wet and/or reactive plasma etching process was implemented for all-refractory junction patterning.

(c) Reference junctions with Nb, $Nb_3Sn$, and Mo-Re base electrodes and soft alloy, Pb-Bi, counterelectrodes have been fabricated with excellent quasiparticle I-V characteristics when using the $Al/Al_2O_3$ overlayer barriers.

(d) A dependence of the subgap leakage current upon the barrier crystallinity (texture) was discovered. Only sputtered $Al/Al_2O_3$ barriers worked well on Nb whereas evaporated $Al/Al_2O_3$ was equally effective on $Nb_3Sn$.

(e) All-refractory junctions with Nb or $Nb_3Sn$ base and Nb counterelectrodes invariably exhibited a high subgap leakage current. This was tentatively attributed to the presence of electronic states at the barrier/protective-Al-overlayer interface, again related to the epitaxial growth of the $Al/Al_2O_3/Al/Nb$ layered structure. Current work is concentrated on this problem.

(f) Properties of sputtered and UHV-evaporated Mo-Re films were determined and compared. The UHV-evaporated Mo-Re was found to be an ideal material for counterelectrodes with a $T_c$ of 12K.

# 2. EXPERIMENTAL APPARATUS AND METHODS

## 2.1 Film Deposition

All thin films which have been studied have been deposited in the Westinghouse Superlattice Deposition and Analysis Facility (SDAF). The schematic of the SDAF configuration is shown in Figure 2.1. A description of the facility is given in Reference 1. Films of Nb, $Nb_3Sn$, and Mo-Re have been evaporated and films of $V_3Si$ and Mo-Re were sputtered. Metallic overlayers 20-60 A thick which were oxidized for use as tunnelling barriers were deposited by both techniques.

The evaporation chamber of the SDAF had a pressure in the low $10^{-11}$ torr range with its cryopanels cold. The chamber has been opened to atmosphere about once a month for maintenance. The background pressure during deposition (sources at high temperature) ranged from $3x10^{-9}$ torr during the first week after a pumpdown and bakeout cycle to $3x10^{-11}$ torr during later weeks.

Fine control of evaporation rates was not important for single-element films. Quartz-crystal thickness monitors were used to measure the accumulated thickness. However, for $Nb_3Sn$, the Sn rate had to be controlled by a PID feedback control of effusion cell temperature. The feedback loop for Nb evaporation rate control used the signal from an Inficon Sentinel rate monitor to control the emission current of the electron-beam source. In the case of Mo-Re films, the Mo evaporation rate was again controlled by the Sentinel whereas the Re rate was controlled by using a rate signal derived from a crystal monitor and acting on the e-beam source emission current. Deposition rates were 1 to 5 A/sec.

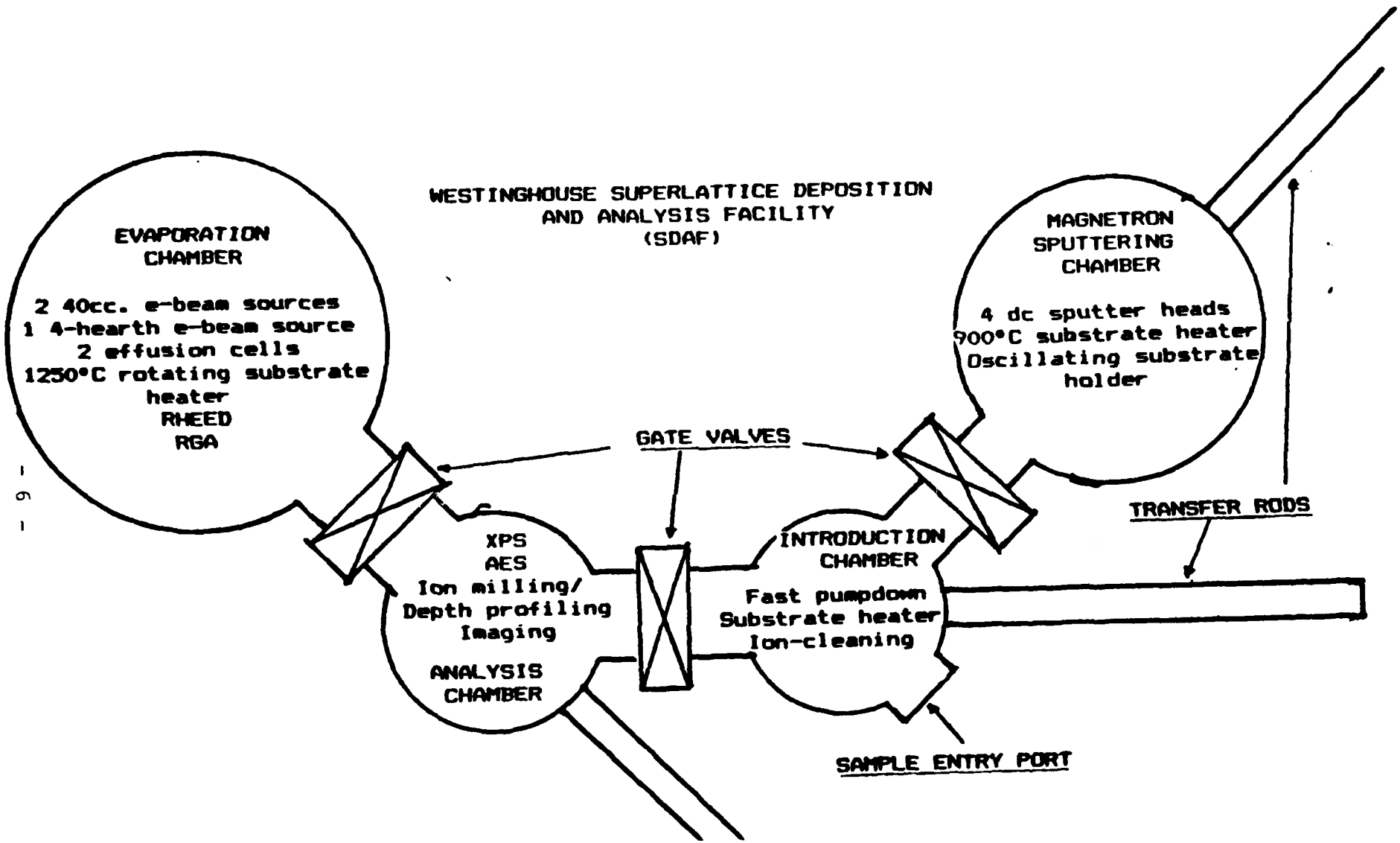


Figure 2.1 Schematic of the current status of the SDAF.

for superconductors and 0.1 to 0.5 A/sec. for barrier materials. The substrates were rotating at 23 rpm so that, for barriers, less than a monolayer was deposited during each revolution.

Sapphire substrates were used with an epitaxial-grade polish. They were clamped to a molybdenum block and degassed in the introduction chamber of the SDAF at 700 $^{o}$C before deposition. The substrate temperature was measured by a W-5%Re/W-25%Re thermocouple inserted into a cavity of the block. The substrate temperatures used for specific experiments will be presented in the next section.

The background pressure in the magnetron sputtering chamber of the SDAF was 6 to 10x10$^{-9}$ torr with the cryopump throttled just before introduction of argon. $V_3Si$ was co-sputtered from single-element targets by oscillating the substrate holder in front of two 2-inch dc magnetron guns spaced 60$^{o}$ apart on the wall of a cylindrical chamber. However, a maximum deposition rate was obtained which was too low. The $T_c$ of films with 24-25 atomic percent silicon grown on an 800$^{o}$C substrate was only about 12K which we attributed to impurities incorporated during the depositions. Attempts to increase the deposition rate have not been made since the results of the XPS study of A15 surface oxidation and atomic segregation indicated that the latter is especially pronounced in $V_3Si$. Consequently, $V_3Si$ turned out to be the least desirable A15 compound for use in high-$T_c$ tunnel junctions. The surface of $Nb_3Sn$ segregated much less, and it was chosen, therefore, to represent stable A15 materials for the balance of this project.

The additional advantage of using $Nb_3Sn$ in this work is the

possibility of co-evaporating a high-quality A15 material while using only one e-beam source (for niobium). The low melting point of tin makes it possible to use an effusion cell with an inherently well-controlled evaporation rate. In the case of $V_3Si$, both elements have to be evaporated from e-beam sources that, at this juncture, have less well-controlled evaporation rates. In recent months, the magnetron sputtering chamber has been used almost exclusively for barrier deposition. A comparison of the properties of sputtered and evaporated barriers will be made in Section 3.

## 2.2 Analytical Methods

X-ray Photoelectron Spectroscopy (XPS) was used extensively for Task 1 during the first year of this project to study the A15 superconductor/barrier oxide interface and identify necessary conditions for effective barrier formation. The results of Task 1 were reviewed in Reference 1. Additional results are reviewed in Section 3. XPS has been used during the last year as a routine indication of reproducibility of overlayer thickness, oxide thickness, protection of the superconductor from oxidation, and the composition of the surface of the superconductor. The measurement of surface composition by XPS was accurate to ±5 atomic percent. Energy Dispersive Spectroscopy (EDS) was used as a measurement of the composition of the bulk of the film.

This project has benefited from the results of a more basic research program cost-shared by Westinghouse and AFOSR (Contract No. F49620-83-C-0035). One of the goals of that program was to characterize the crystalline perfection of A15 surfaces and their

interfaces with barrier materials. The particular tool for such work was Reflective High-Energy Electron Diffraction (RHEED). The most basic application for this program was in the observation of crystalline order in the barrier metal, its oxide, and in a thin counterelectrode. RHEED observations will become more important in the third year of the program when A15 superconductors are deposited as counterelectrodes.

### 2.3 Junction Fabrication from Trilayers formed in situ

During the first year of the project, reference junctions were formed by depositing a superconductor/barrier bilayer without exposing the interface to air. A cross strip of Pb-Bi was deposited in another vacuum system to complete the junction. While this process has been useful each time a new base electrode material has been used or a process modification has been introduced, there were limitations in control of junction size, oxide growth, and cleanliness or chemical state of the barrier/counterelectrode interface.

A simple process with turnaround times of 2-3 days has been developed to delineate junction areas from a trilayer formed completely in the SDAF. A typical "trilayer" consisted of a base electrode deposited in the evaporation chamber, a metallic overlayer formed in the sputtering chamber and oxidized in the introduction chamber in 100 millitorr of pure oxygen, a sputtered layer of the same metal <40 A thick to isolate the oxide from the counterelectrode, and an evaporated counterelectrode.

Figure 2.2a shows the trilayer covering the entire substrate except for the area under the clamps. The junction areas were

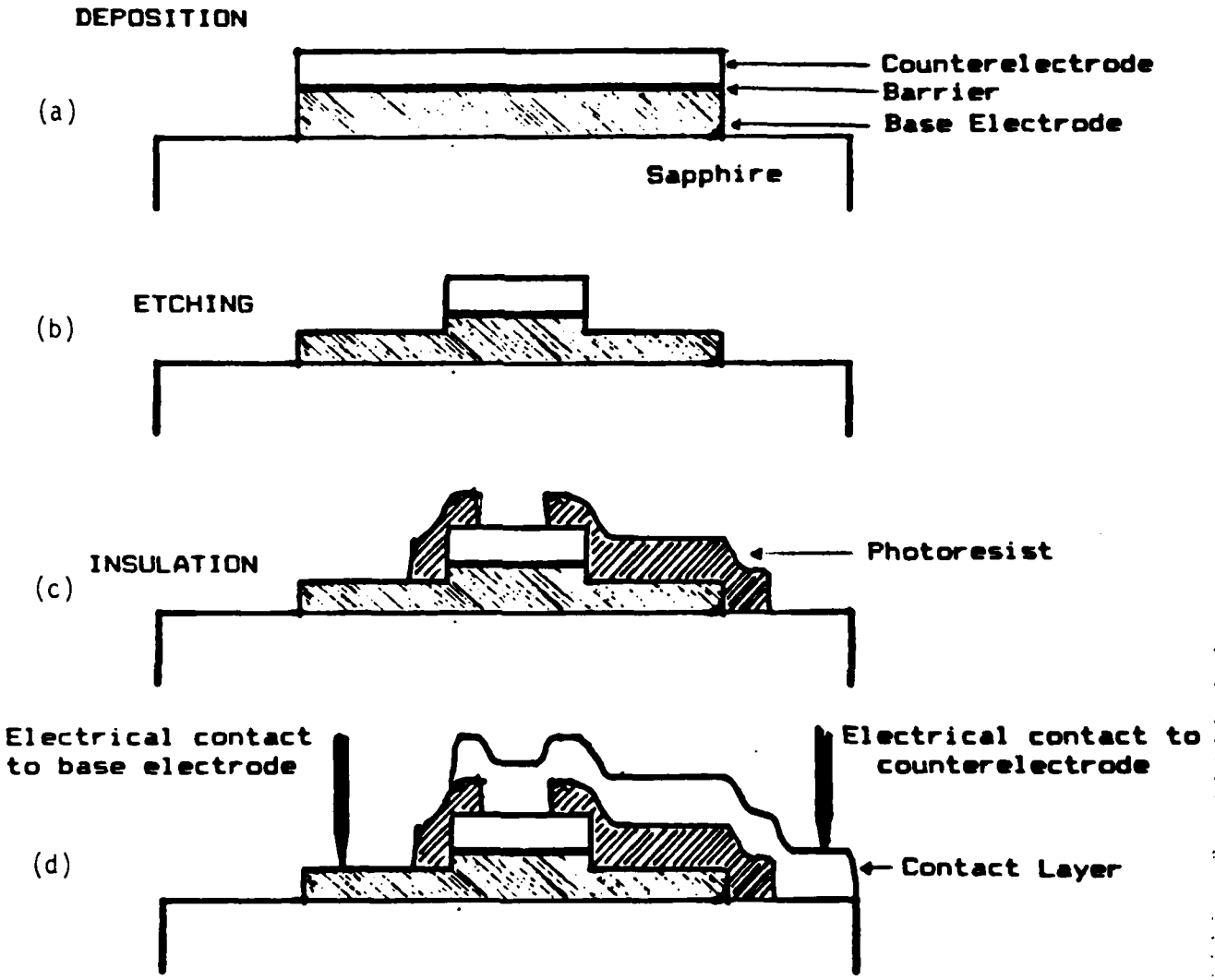


Figure 2.2 Processing steps to form a tunnel junctions from a trilayer formed in situ.

protected with patterned photoresist while the counterelectrode was etched. The etching step has been performed by wet chemistry for fast turnaround. In a separate Westinghouse program, reactive ion etching (RIE) has been used to remove excess material from the top layer. That process will be used during the third year of the project when junction area reproducibility and finer linewidths become important. The etched sample is shown in Figure 2.2b. Although the etching is retarded by the oxide barrier, it may remove some of the base electrode material without harming the junction. The thickness of the remaining film was checked by a Sloan DEKTAK to be sure that the etch removed the top layer completely.

A second layer of photoresist was patterned as shown in Figure 2.2c and left in place to insulate the base electrode from the metallization layer shown in Figure 2.2d making contact to the top electrode.

# 3. RESULTS AND DISCUSSION

## 3.1 Task 1 - Superconductor/Barrier Interfaces

The first annual report issued under this program included a number of XPS measurements of thin metallic overlayers of Al and Y on Nb and $V_3Si$. We will report here on several specific areas which we continued to explore in the second year: diffusion of thin metallic overlayer material into the base, the uniformity of the thickness of thin metallic overlayers, and surface segregation of the components of several A15 compounds upon exposure to oxygen.

There are two remaining topics which are related to these, and which we will continue to study during the third year. The first topic is to simply extend the measurements of diffusion of overlayer material to bilayers with a base of single-crystal Nb and, perhaps, also with a highly-textured high-$T_c$ material. The second topic is to observe the diffusion of both the oxidized and unoxidized parts of the overlayer with XPS at high temperatures. The diffusion rates at elevated temperatures are a crucial part of the background information needed for the next step in Task 4, the fabrication of $Nb_3Sn$ counterelectrodes.

### 3.1.1 Diffusion of Thin Metallic Overlayers

Kwo et al. observed that the thicknesses of thin (10-40 A) Al overlayers on Nb determined by XPS were less than the nominal thicknesses based on sputtering rates.[2] The difference was ascribed to grain boundary diffusion. Additional data collected under this program for Nb/Al bilayers is shown in Figure 3.1a and

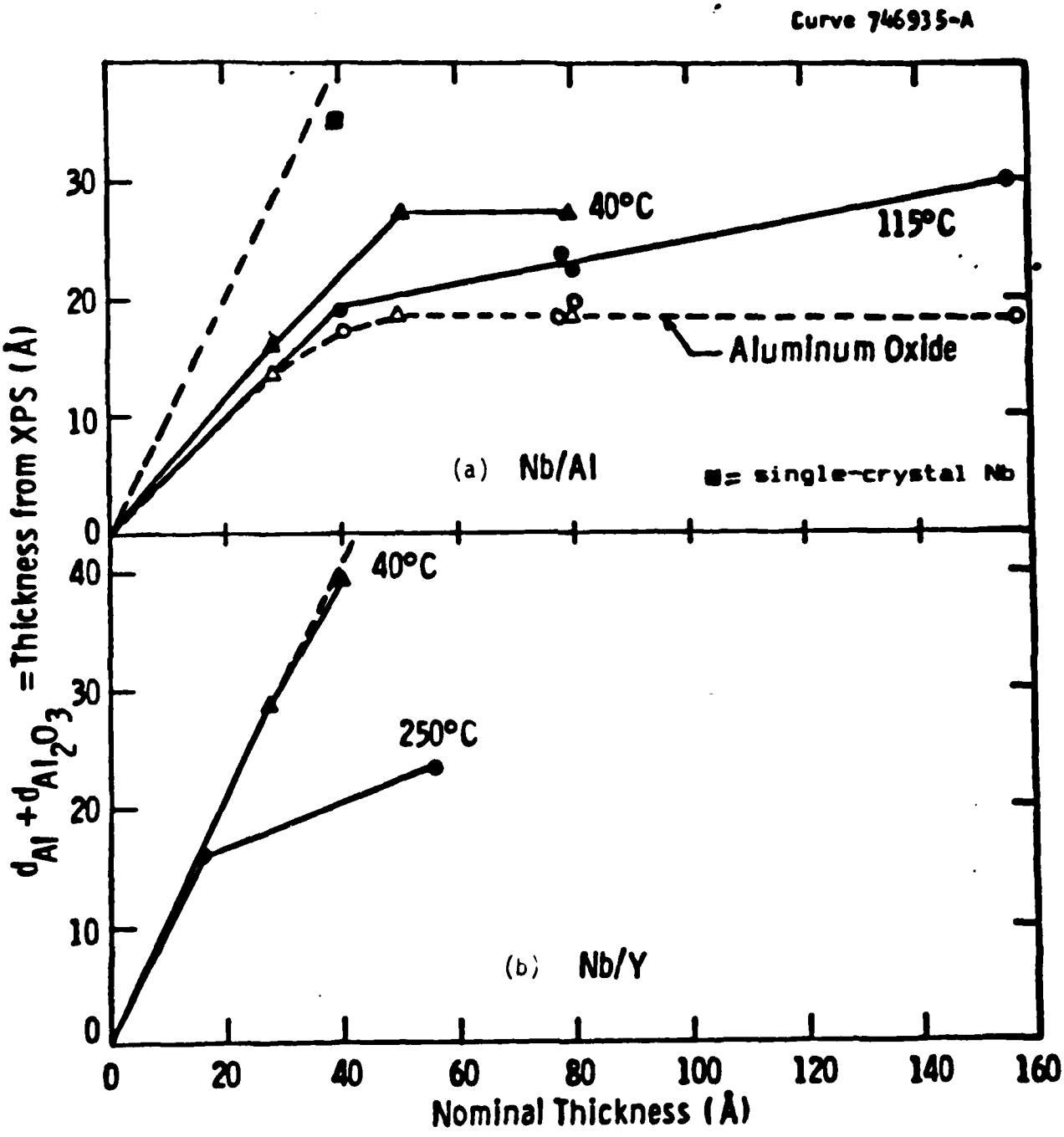


Figure 3.1 The thicknesses of oxidized aluminum and yttrium overlayers deposited on Nb compared with the nominal thicknesses based on deposition rates. The dashed line indicates agreement btween the measured thickness and the nominal value.

new data on Nb/Y bilayers is shown in Figure 3.1b. For the samples in Figure 3.1a, the measured Al + $Al_2O_3$ thickness was always less than the nominal value with a discrepancy that was greater at a 115°C deposition temperature than at 40°C. The aluminum oxide thickness was constant at 18-20 A because all samples were exposed to air for approximately 10 minutes.

The Y overlayers deposited at 40°C had a thickness which agreed well with the nominal thickness. However, there was some diffusion of Y into the Nb base for a 250°C deposition. The Nb base used for this series of measurements was polycrystalline. Based on Kwo's report that the diffusion rate was lower for a polycrystalline sample with larger grains, we expect that there will be little or no loss of overlayer material by diffusion into single-crystal Nb at temperatures below 500°C. The one point in Figure 3.1a obtained for Al deposited at 25°C on single-crystal Nb tends to support this expectation.

Figures 3.2a and b show the results of thickness measurements by XPS compared with nominal thicknesses for overlayers of Al and Y on $V_3Si$. Comparison between Figures 3.1a and 3.2a shows that there was less of a tendency for Al to diffuse into $V_3Si$ at 250°C than into Nb at 40°C. Yttrium also tended to diffuse more slowly into $V_3Si$ than into Nb according to the data in Figures 3.1b and 3.2b. The yttrium oxide thickness was fairly constant at 40-45 A thick because the exposure to air was about 10 minutes for all samples.

### 3.1.2 Uniformity of Overlayer Thickness

Measurements of overlayer thickness reported in Figures 3.1

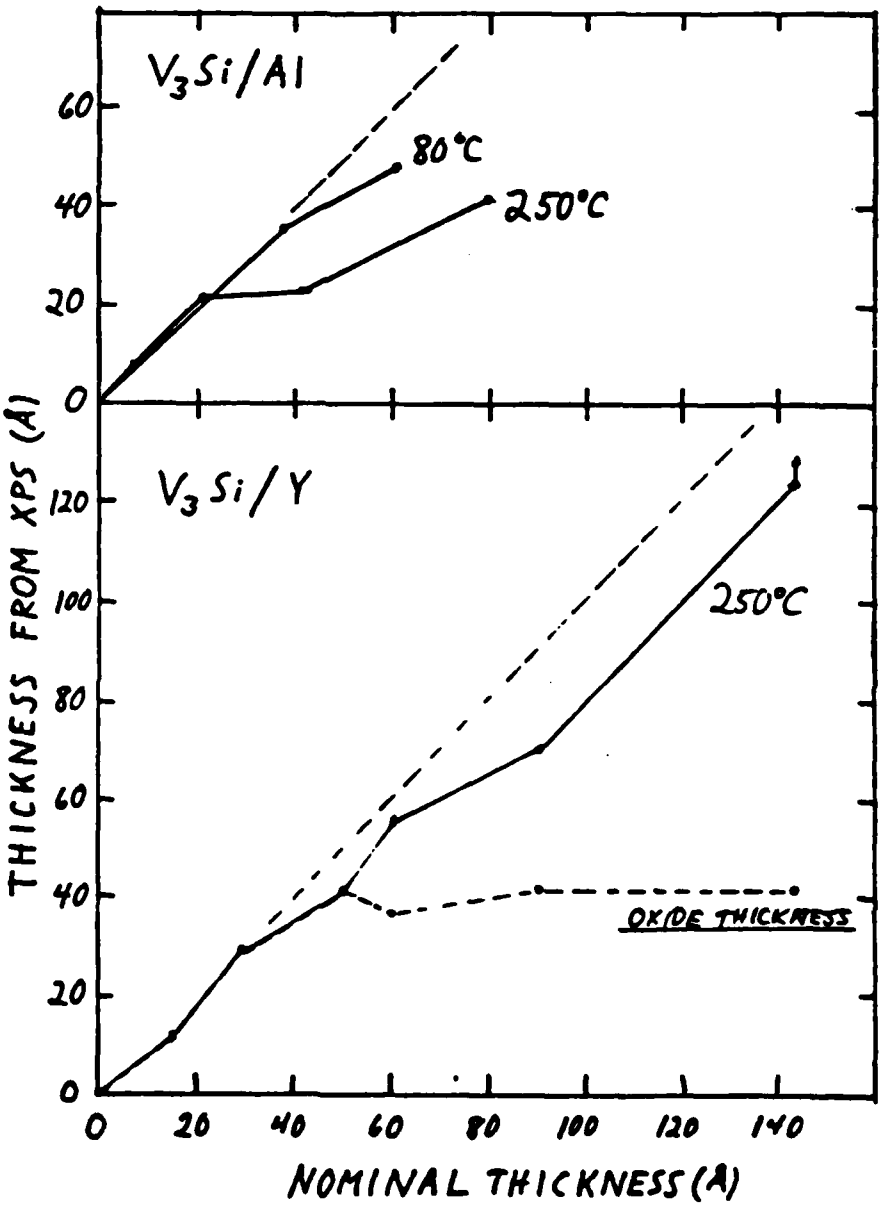


Figure 3.2 The thicknesses of oxidized aluminum and yttrium overlayers deposited on $V_3Si$ compared with the nominal thicknesses based on deposition rates.

and 3.2 were recorded with the electron-energy spectrometer positioned normal to the surface of the samples. Measurements have been made with the angle between the spectrometer and the normal to the sample, $\theta$, set at a series of values. The distance which an electron emitted at a certain distance below the surface of the film must travel to escape the film is increased by a factor of $1/\cos\theta$. This factor has been included in the data shown in Figure 3.3 so that the normalized barrier thickness would be 1.0 for all values of $\theta$ for a smooth overlayer of uniform thickness. However, the thickness of all overlayers measured seemed to decrease as $\theta$ increased indicating that either the substrate (bottom layer) was rough or that the overlayer was deposited on a smooth layer but did not have a uniform thickness.

Grundner has modeled both cases for thickness variation with $\theta$. [3] His plot of thickness versus $\theta$ for a uniformly-thick overlayer on a rough surface is reproduced in Figure 3.4 for a series of roughness parameters. The parameter which determined the extent of roughness was the ratio of the amplitude to the period of the sinusoidal surface he used.

Grundner's model for non-uniform thickness had a Gaussian distribution of thickness. His plot with $\sigma = 1.0$ is reproduced in Figure 3.3 where it is represented by solid circles. The experimental points in Figure 3.3 followed curves which looked much more like the one derived from a model of non-uniform thickness than from a model of a rough surface. In particular, the data points shown as open squares followed the model best. Those points were from measurements of an amorphous Si overlayer deposited on an extremely smooth amorphous MoGe film supplied to

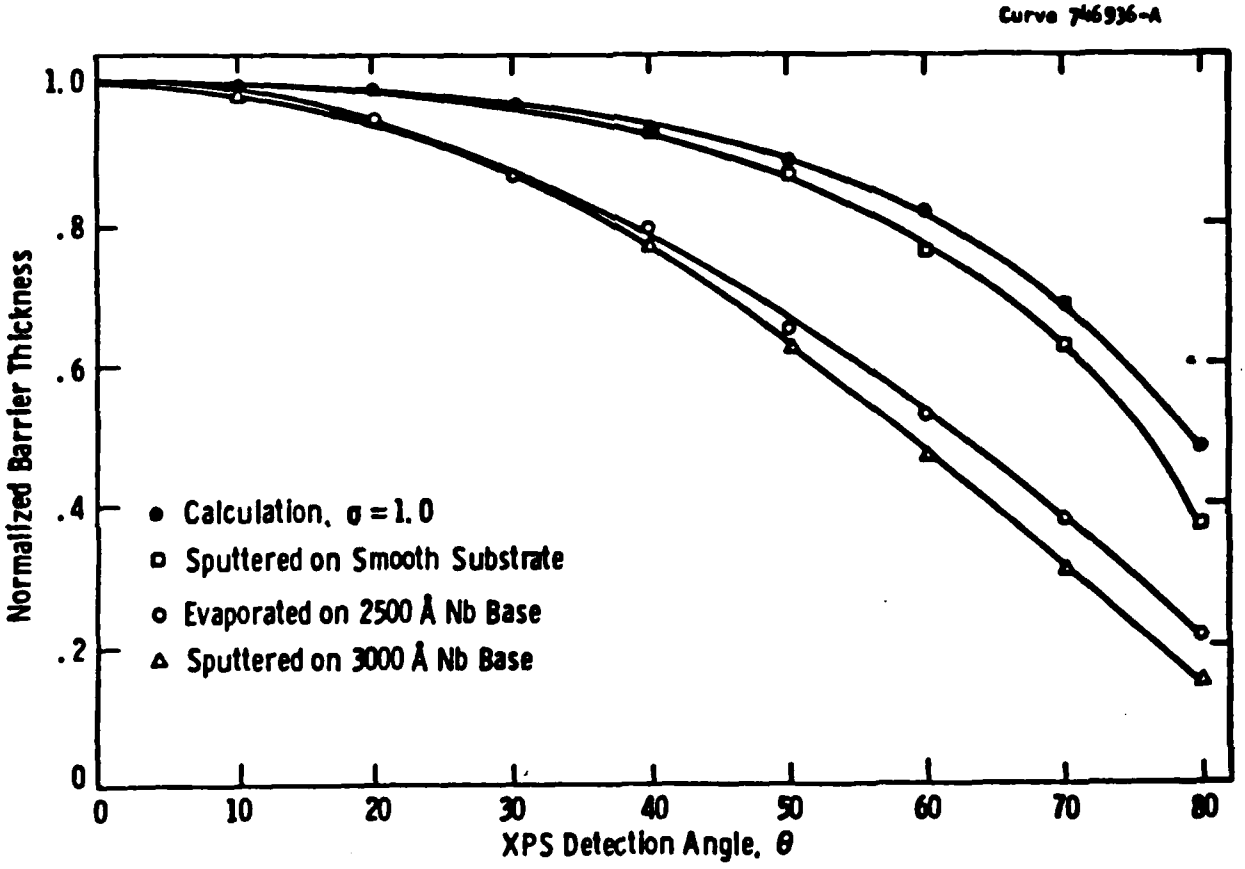


Figure 3.3 The normalized thicknesses of three overlayers determined by XPS at a series of detection angles compared with the apparent thickness of an overlayer modeled as having a Gaussian distribution of thickness and $\sigma = 1.0$.

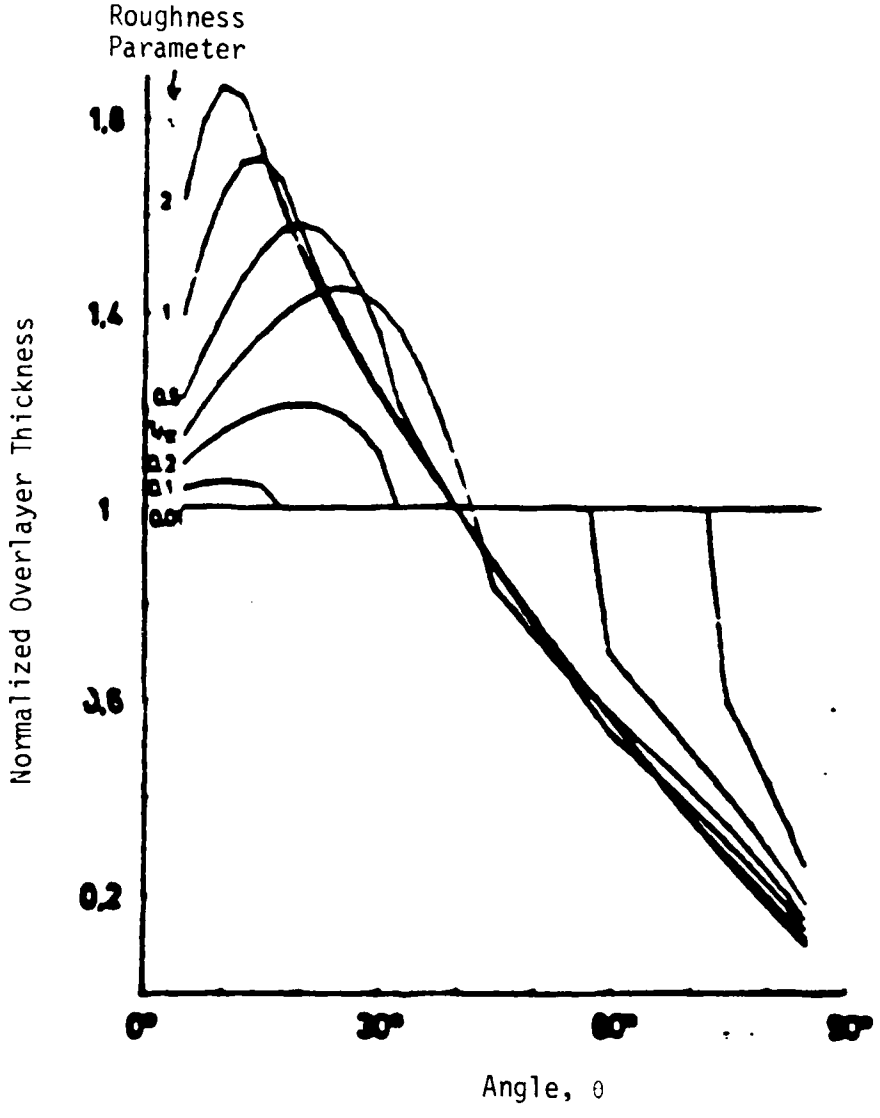


Figure 3.4 The apparent thickness of an overlayer with a uniform thickness of 1.0 which is on a rough surface. The substrate is modeled as a sinusoid with a roughness parameter defined as the ratio of the amplitude to the period of the sinusoid.

us by J. Graybeal of Stanford University for this purpose.[4] The other data points, from Al overlayers either evaporated or sputtered on a polycrystalline Nb base, had a greater decrease in the apparent thickness for $\Theta < 40^{\circ}$ indicating that the rough substrate had some influence. However, the curves more closely resemble the curve derived from a non-uniform thickness of the overlayer.

The data for Nb/Al bilayers were typical of the dependence of the apparent thickness of overlayers with XPS detection angle for Al, Y, and Si overlayers on $V_3Si$, $Nb_3Sn$, $V_3Ga$, and polycrystalline Nb. The exceptions were for thin overlayers deposited on single-crystal Nb which had a ratio of normalized thickness, $d(\Theta=80^{\circ})/d(0) = .4$, indicative of a smoother Nb surface.

The use of $\sigma = 1.0$ in the model of thickness non-uniformity corresponded to fluctuations in the thickness of overlayers (tunnelling barriers) comparable to their thickness. This clearly overstates the extent of the non-uniformity for three reasons.

1. Thin metallic overlayers have been observed by XPS to completely protect highly reactive underlayers such as Nb from oxidation while the surface of the bilayer was exposed to air.

2. The leakage current at zero bias in tunnel junctions formed by adding a Pb-Bi counterelectrode to a bilayer was a very sensitive probe of pinholes in the barrier but was low for a number of base/barrier combinations. For base electrodes of Mo-Re, in particular, any point at which the barrier thickness was zero would be a superconducting short because Mo-Re

surfaces only formed a 2 A thick oxide.

3. A comparison was made between the oxide thickness measured by XPS and a thickness inferred from a fit to the .1-.4 volt region of the tunneling current-voltage curve following Simmons.[5] The electrical measurement gave an average weighted toward the thinnest spots in the barrier. The thickness from XPS was typically 4-5 A greater than from the Simmons' model. Typical figures for $Al_2O_3$ were 20 A versus 16 A. For $Y_2O_3$, typical values were 45 A versus 41 A.

### 3.1.3 Segregation of A15 Compounds

Ihara et al. have shown qualitatively using X-ray Photoelectron Spectroscopy (XPS) that an atomic segregation of the constituents of an A15 compound occurred when the surface was oxidized.[6] Our data for $Nb_3Sn$, $V_3Si$, and $V_3Ga$ are shown in Table 3.1. The compositions listed in Table 3.1 which were derived from XPS measurements were based on elemental sensitivities compiled by the analyzer manufacturer modified by our own measurements of elemental standards.

The entries in Table 3.1 for each A15 compound were ordered by increasing thickness of the oxidized A15 layer. The oxidation occurred either because there was no barrier or a very thin one, or in some cases because there was some exposure to oxygen before barrier deposition. The column which lists the percentage of B element oxide shows the extent of segregation which occurred during oxidation. It is the number density of B atoms in an oxide environment compared with the total number of A and B atoms which emit photoelectrons with a chemical shift characteristic of the

| Compound $A_3B$ | Sample # | Barrier Thickness (Å) | Oxidized A15 | | A15 Metal | |
|---|---|---|---|---|---|---|
| | | | Thickness (Å) | % B Oxide | at. % B (XPS) | at. % B (bulk) |
| $V_3Si$ | 9-B5 | 100 | 0 | -- | 24 | 27 |
| | 3-B5 | 37 | 2 | 100 | 30 | 30 |
| | 4-B5 | 20 | 9 | 100 | 80 | 35 |
| | 8-B2 | 0 | 73 | 62 | 47 | 29 |
| | 8-B4 | 0 | > 100 | 72 | -- | 29 |
| $Nb_3Sn$ | 18-B5 | 50 | 0 | -- | 21 | 21 |
| | 33-B6 | 26 | 4 | 48 | 31 | 26 |
| | 13-B4 | 0 | 33 | 39 | 23 | 23 |
| $V_3Ga$ | 138-A10 | 20 | 0 | -- | 23 | 23 |
| | 114-A1 | 25 | 0 | -- | 22 | 21 |
| | 114-B1 | 25 | 11 | 45 | 22 | 29 |

Table 3.1 Surface segregation of A15 compounds.

oxide. By this definition, an $A_3B$ compound which was completely oxidized would have an entry of 25%.

When $V_3Si$ oxidized, $SiO_2$ formed first and a number of samples have also shown an increased silicon concentration in the metal underneath. There must have been a V-rich layer left behind which would be deep enough compared to the coherence length of 40 A to affect tunneling properties. Sample 8-B4 had an oxide layer which was too thick to measure because it was dipped in water and left to dry in air.

The segregation of $Nb_3Sn$ was less dramatic than for $V_3Si$. $Nb_2O_5$ forms at the same time as $SnO_2$ but in a concentration less than 75%. In contrast to $V_3Si$, no change in the composition of the superconductor at the interface with its oxide was observed within the resolution of our measurements, which is consistent with the fact that excellent tunnel junctions have sometimes been made with the native oxide of $Nb_3Sn$.[7] Nevertheless, we observed higher subgap currents in tunnel junctions with some base electrode oxidation due to exposure to humid air.

The $V_3Ga$ samples were deposited at Stanford. They had surface compositions similar to the bulk except for the sample with 11 A of oxide growth. The oxide layer was deficient in vanadium oxide and the adjacent superconductor showed a small increase in Ga concentration. Junctions formed on samples 114-A1 and B1 had similar characteristics. However, the XPS measurements were made after the counterelectrode and insulator layers were stripped in acetic acid and acetone so oxidation of the $V_3Ga$ probably occurred only after the junctions were measured.

The importance of avoiding the deleterious effects of A15

oxidation is analogous to the same need for Nb-based junctions. We observed a degradation of tunneling characteristics when Al barriers were too thin to protect underlying Nb base electrodes or when some oxidation occurred before the Al was deposited, in agreement with a number of others such as Wolf.[8] However, the mechanism which leads to a weakly superconducting surface layer in several A15 materials is an atomic segregation rather than the suboxide formation that occurs at a niobium/niobium oxide interface.

### 3.2 Task 2 - Analogue to SNAP Process

Task 2 of the work statement specified the development of a selective anodization process for A15 films. This task was formulated based on an analogy with the Selective Niobium Anodization Process (SNAP) developed at Sperry Research Center for Nb/Si/Nb junctions.[9] As we mentioned in the first annual report, some process for patterning a base/barrier/counterelectrode trilayer formed *in situ* such as the one described in Section 2.3 of this report is needed. A process based on etching rather than anodization was used for several reasons.

1. Private information obtained from Sperry at the beginning of the program made it clear that anodization does not work well for Nb-based compounds such as NbN.

2. At the same time, a successful demonstration of trilayer patterning by plasma etching of Nb (SNEP) was reported by Bell Laboratories.[10]

3. Parameters of an etching process are generally less sensitive

to the type of material processed. We have successfully patterned trilayers with counterelectrodes of Nb and Mo-Re, and have experience with reactive ion etching and wet chemical etching of Nb-based A15 compounds.

Wet chemical etching has been performed with a solution of deionized water, $HNO_3$, and HF in proportions of 20:9:1, which was left to stabilize at room temperature for 15 minutes after mixing. Polycrystalline $Nb_3Sn$, Nb and Mo-Re all etched at a rate of about 30 A/sec. Single-crystal niobium etched at a rate of only 3 A/sec. The etching rate of oxide tunnelling barriers was not measured directly but was inferred to be much slower. DEKTAK thickness measurements performed after etching for a length of time which should have etched through the entire counterelectrode and several hundred Angstroms of base electrode material often showed that the etching had stopped at a thickness corresponding to the base electrode plus barrier thickness.

RIE rate calibrations were done only for trilayers with polycrystalline Nb electrodes and $Al_2O_3$ barriers. Trilayers were etched in an Anelva reactive ion etch system in a total gas pressure of 30 millitorr at a power of 150 W ( 0.125 W/cm$^2$). $CCl_4$ or $CCl_4$+30% Ar were used to etch through the entire trilayer down to the substrate at a rate of 350 A/min. Pure $CF_4$, with an etch rate of 250 A/min., was used when it was desirable to stop the etching at or just below the barrier. The difference in the behavior of the etches at the barrier was due to the difference in volatility of $AlCl_3$ and $AlF_3$. $AlCl_3$ has a vapor pressure of 1 torr at only 100$^o$C whereas $AlF_3$ must be heated to 1238$^o$C to have an equal vapor pressure, so $AlF_3$ can only be removed by the

physical sputtering component of RIE.[11] $CF_4$ has been a suitable etching gas for films of Nb-based A15 materials so it will be used for etching trilayers with $Nb_3Sn$ electrodes.

Progress in Task 2 has been sufficient to establish a reliable processing of junctions using the procedure described in Section 2.3.

At this juncture, there is no identified need for any additional work: the goal of Task 2 was attained. During the third year of the program, however, additional work may be required if new RIE equipment becomes available.

### 3.3 Task 3 - Reference Junctions

Tunnel junctions have been fabricated with the low-$T_c$ materials, Nb and Pb-Bi, as base or counterelectrodes to achieve the following goals which specifically affect the fabrication of high-$T_{op}$ tunnel junctions.

1. Show that complete coverage of the base electrode by the barrier and protection of the base electrode from oxidation (as indicated by XPS) were actually achieved.

2. Dismiss concerns about chemical interactions between the barrier and base electrode materials which would reduce the $T_c$ of the surface layer.

3. Allow a more complete characterization of the barrier through tunnelling resistance above the gap, leakage currents at zero bias, Josephson current, and barrier height and width from Simmons' model.[5]

4. Determine the homogeneity of the superconductors within a coherence length of the barrier. If one electrode (Pb-Bi, Nb) is assumed to be homogeneous and the barrier has low leakage, then excess conductance above the gap voltage can be attributed to a distribution in the value of the gap of the other electrode.

### 3.3.1 Nb-based Junctions with Pb-Bi counterelectrode

The standard oxidation procedure was to expose the samples to 100 millitorr of dry $O_2$ in the introduction chamber of the SDAF for 1 hour. In the particular case of Pb-Bi counterelectrodes, the samples were removed from the SDAF and were exposed to atmospheric (necessarily humid) air for about 10 minutes while an insulating polymer coating was painted on to define junction areas, and the samples were transported to a separate vacuum system for Pb-Bi evaporation. We do not know whether the exposure to moisture after the dry oxidation played a role in the oxidation rate or affected the tunnelling properties. However, the exposure to humidity has been found by Ronay and Latta to be crucial to low-leakage yttrium oxide barriers when a Nb counterelectrode was used.[12] The issue will be discussed further in Section 3.3.4.

The quasiparticle current-voltage characteristics (I-V) of four tunnel junctions with oxidized Al barriers are shown in Figure 3.5. Each barrier was structurally different from the others and had a leakage current which depended on the structure. No differences between these junctions appeared in XPS studies of the oxidized Nb/Al bilayers. All had a layer of $Al_2O_3$ approximately 20 A thick, a layer of unoxidized Al underneath which

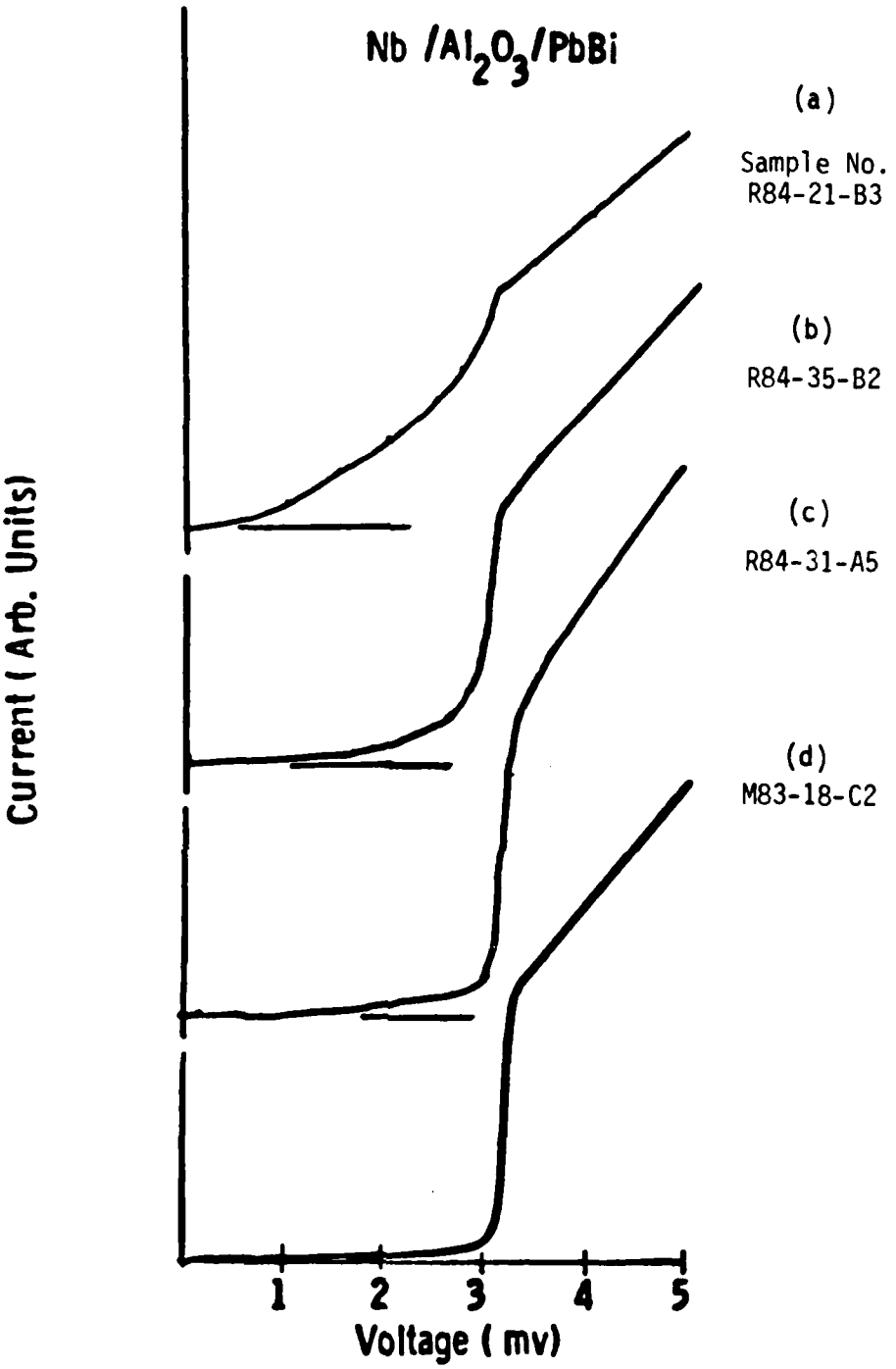


Figure 3.5 The quasiparticle I-V characteristics of four Nb/oxidized Al/PbBi tunnel junctions with barriers of different morphologies. a) Highly-textured evaporated Al b) Amorphous barrier after ion-milling c) Highly-textured sputtered Al d) Randomly-oriented fine-grained Al grown on sputtered polycrystalline Nb.

was less but not much less than 10 A thick, and a Nb surface which showed no signs of oxidation - even with the XPS spectrometer at a glancing angle.

The evaporated Al overlayer (3.5a) and sputtered Al overlayer (3.5c) were grown on a single crystal Nb (resistivity ratios up to 150) surface and both were highly textured according to their RHEED patterns. The sample used for Figure 3.5a represented repeated experiments with the same high leakage in all cases. The sample used for Figure 3.5b was ion-milled after oxidation which made the oxide amorphous and reduced the leakage current. The samples were exposed to an argon ion beam with an energy of 600 V. and current density of 250 nA./cm.$^2$ for 15 minutes. There was no measurable loss of aluminum oxide from ion-sputtering as determined by XPS. Figure 3.5d shows the I-V curve from a sample with a sputtered Al overlayer on a polycrystalline Nb base. The RHEED pattern had concentric polycrystalline rings and the tunneling properties were nearly ideal.

The influence of the structure of the barrier is being examined as part of the cost-shared Westinghouse-AFOSR program. At present, the role of the texture of the metallic overlayer and the effect of the deposition method (sputtering or evaporation) are not understood. The conclusion we reached in regard to this program was that, despite the minor inconvenience of moving samples within the SDAF, overlayers which were to be oxidized for barriers would be sputter-deposited even if the base electrode was evaporated.

### 3.3.2 Nb-Sn Junctions with Pb-Bi Counterelectrodes

One attempt was made initially to evaporate an Al overlayer on $Nb_3Sn$ despite the problems encountered with these barriers on Nb. The evaporated barriers worked so well that we continued to use evaporated overlayers for junctions with $Nb_3Sn$ base electrodes. The $Nb_3Sn$, the unoxidized Al overlayer, and the $Al_2O_3$ barrier all have had RHEED patterns of highly-textured material. The I-V curve of a typical junction is shown in Figure 3.6a. The junctions were comparable in several ways to those produced at Stanford with oxidized amorphous silicon barriers.[13] The width and midpoint of the $Nb_3Sn$ gap were the same and the excess currents at 3mV were comparable. However, a close inspection of the low voltage part of the curve showed that our junctions generally had a higher leakage at zero bias whereas the Stanford junctions had a higher excess conductance due to inhomogeneity of the surface layer of the $Nb_3Sn$. It is not clear why evaporated, highly-textured $Al/Al_2O_3$ formed low-leakage barriers on $Nb_3Sn$ and not on Nb.

Figure 3.6b shows the quasiparticle characteristics of a $Nb_3Sn$ sample with an evaporated and oxidized yttrium barrier. The $Y_2O_3$ barrier was about 45 A thick as determined by XPS and by fitting the 0.1-0.4 volt region of the I-V curve with Simmons' parameters. The thick oxide resulted in a high resistance above the gap, $R_n$, of $2x10^2$ ohm-cm$^2$. Aluminum oxide barriers were about 20 A thick from XPS and Simmons' parameters with $R_n$ corresponding to more practical values of $2x10^{-2}$ ohm-cm$^2$. The thickness of the yttrium oxide can be controlled by <u>in situ</u> oxidation and counterelectrode deposition but could not be controlled when the samples had to be carried to another vacuum system for Pb-Bi

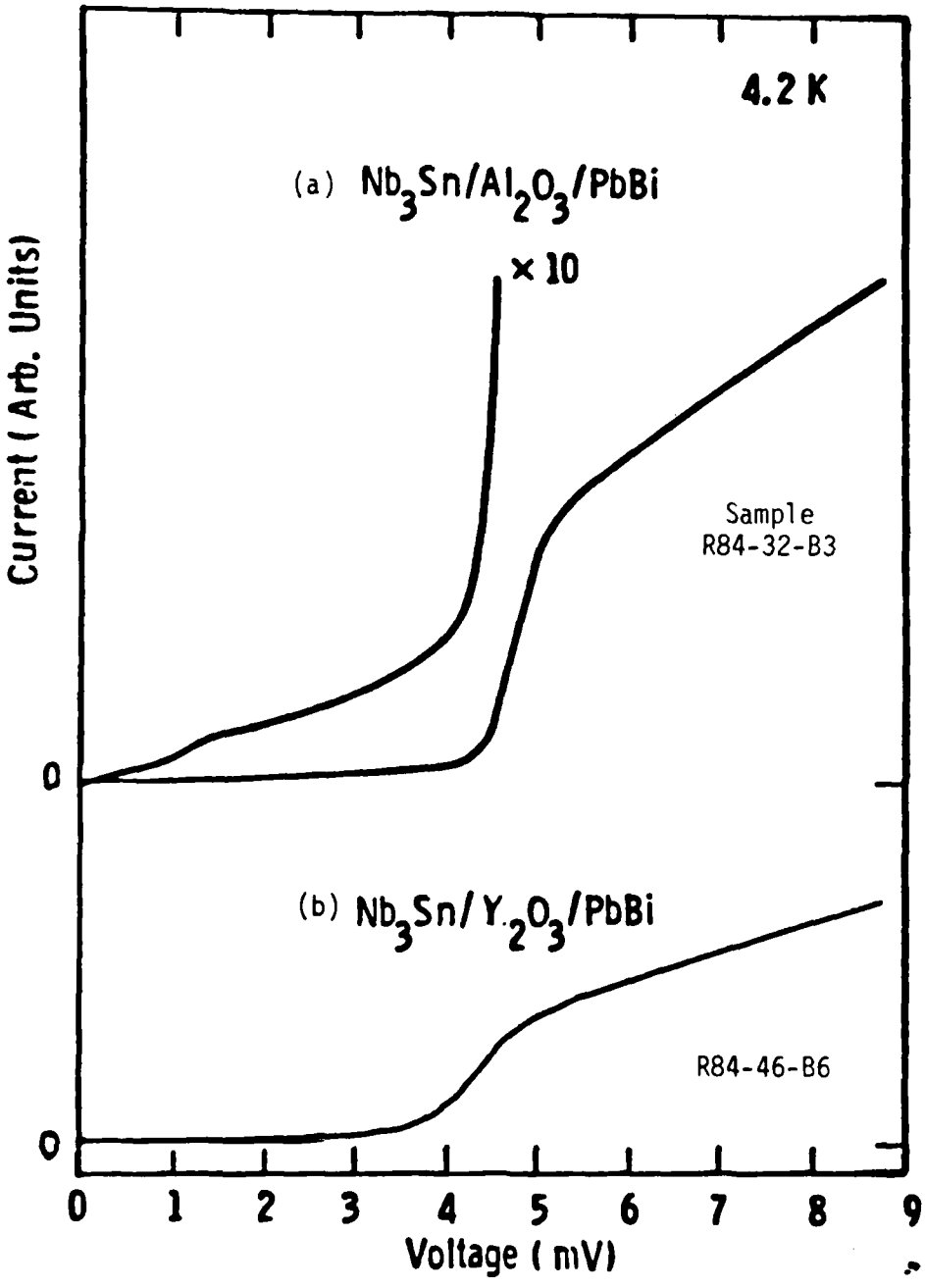


Figure 3.6 The quasiparticle I-V characteristics of two $Nb_3Sn$-based junctions. a) Evaporated (oxidized) Al barrier b) Evaporated (oxidized) Y barrier.

deposition.

### 3.3.3 Mo-Re Tunnel Junctions with Pb-Bi Counterelectrodes

An I-V characteristic of a Mo-Re/sputtered Al(oxidized)/Pb-Bi junction is shown in Figure 3.7. The important features of this curve were the low leakage currents, a sharp rise at the gap corresponding to a $T_c$ = 11.8K, and a proximity-effect "knee" just above the gap. The Mo-Re base electrode was only 200 A thick and there was an unoxidized Al layer determined by XPS to be 13 A thick under the 20 A thick $Al_2O_3$ barrier. Such a thin normal layer (13 A) has not resulted in such an obvious feature due to the proximity effect on thicker base electrodes of Mo-Re or any other material. The sharp rise at the gap voltage shows that the base Mo-Re was homogeneous with a $T_c$ = 11.8K even in such a thin layer. More features of the superconductivity of Mo-Re will be presented in section 3.4.

### 3.3.4 Junctions with Nb Base and Counterelectrodes

The I-V characteristic of a typical Nb/Al(oxidized)/Nb tunnel junction formed *in situ* and later processed with the procedure explained in Section 2.3, is shown in Figure 3.8. The high leakage current was found initially in junctions which had evaporated Al layers which were highly textured. As we have described in Section 3.3.1, such barriers were characterized by high leakage currents for Nb based junctions even with Pb-Bi counterelectrodes. Since low-leakage junctions were obtained when sputtered barriers were used, we have sputtered the Al barriers for subsequent fabrication of junctions with all-Nb electrodes.

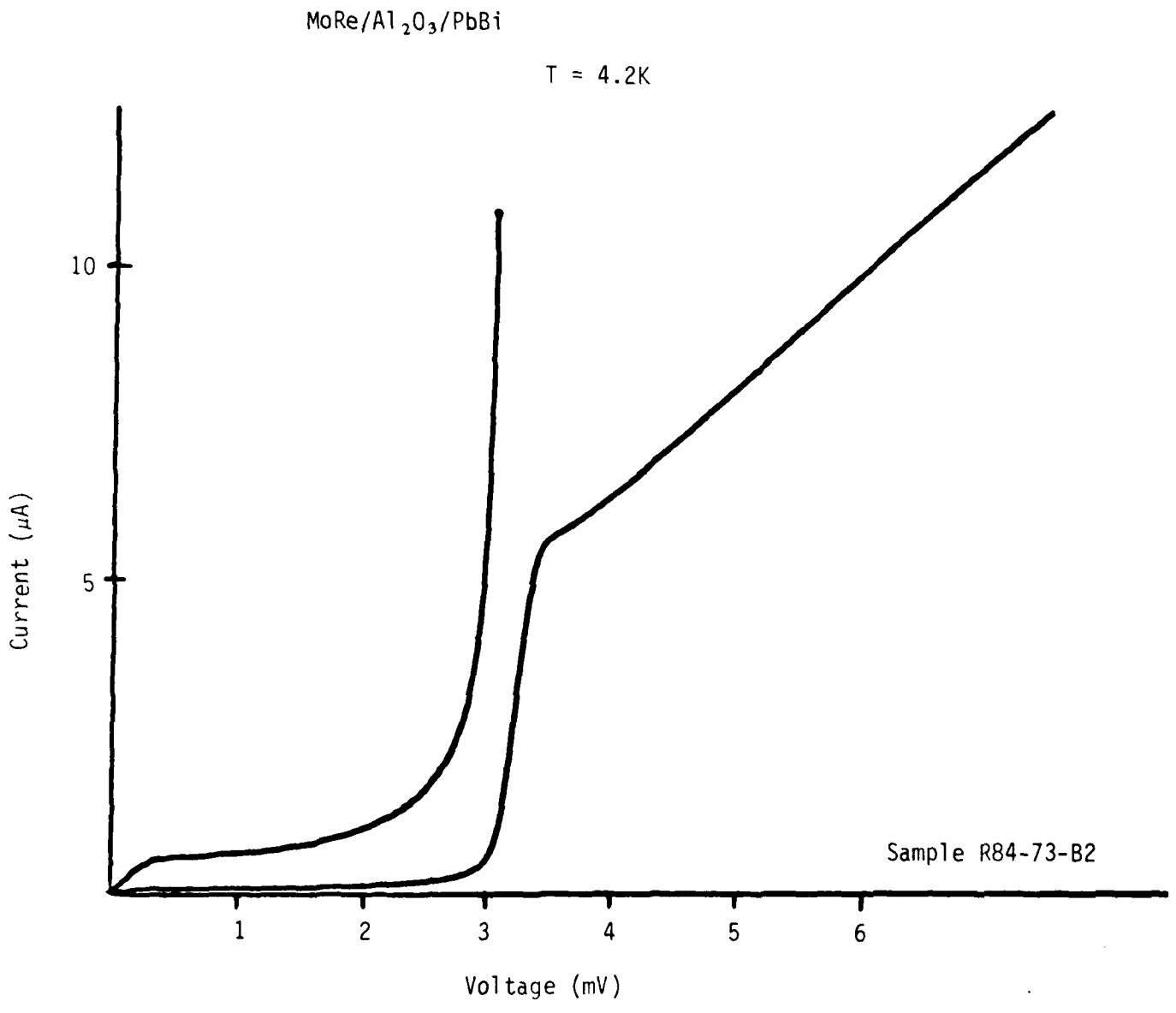


**Figure 3.7** The I-V curve of a junction with a 200 Å thick $Mo_{65}Re_{35}$ base electrode, an oxidized Al barrier, and a PbBi counterelectrode.

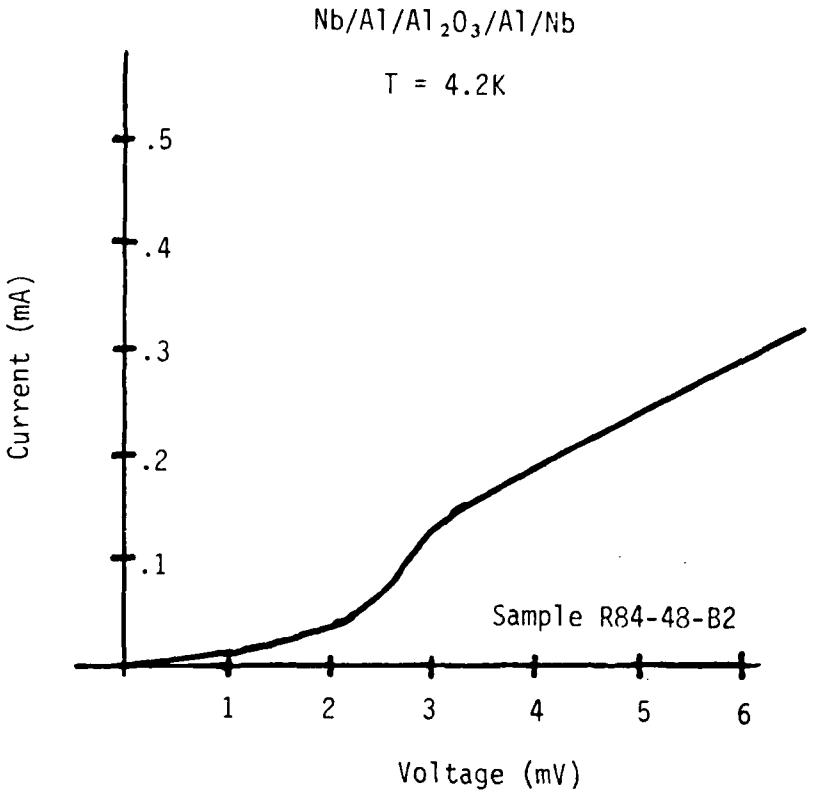


**Figure 3.8 The I-V curves typical of all-Nb tunnel junctions.**

However, in contrast to the results obtained with Pb-Bi counterelectrodes, there was essentially no improvement in the junction characteristics of all-Nb junctions when sputtered barriers replaced evaporated barriers. The I-V curve in Figure 3.8 is that of a junction with a barrier region formed from a sputtered Al layer 40 A thick which was oxidized, followed by a second sputtered Al layer 40 A thick. At the suggestion of M. Gurvitch, we have experimented with exposing the oxidized barrier to moisture before the second Al and Nb depositions but there has been no improvement of the tunneling characteristics.

To simulate the first 200 A to be deposited as a counterelectrode, we evaporated a 200 A thick Nb film at room temperature on a 40 A thick buffer layer of Al on sapphire. Although the film thickness was less than half the coherence length of Nb, the $T_c$ was 8.6K and resistivity ratio was 3.2, so the counterelectrode should have a gap voltage nearly as high as the base.

High confidence in the reliability of the results obtained with Pb-Bi counterelectrodes makes us believe that the high subgap leakage observed here was related to electronic states of the interface between the textured (even if sputtered) barrier and the, presumably, epitaxial protective Al overlayer.

We thus have several experiments planned to modify the barrier including ion milling after oxidation to destroy the highly-textured crystallinity. The highly-textured nature of the overlayers will also be modified by using polycrystalline base electrodes in place of the single-crystal Nb we have employed.

Alternatively, it is possible that the protective Al over-

layer did not cover the $Al_2O_3$ completely. The $Al_2O_3$ formed at room temperature might be less stable than the sapphire used in the last experiment (200 A thick Nb) so that conductive Nb suboxides might have formed in the Nb counterelectrode. This problem is peculiar to Nb so experiments with Mo-Re counterelectrodes which come under Task 5 (Section 3.5) will proceed in parallel with Nb counterelectrodes.

The measurement of the Josephson current will be an additional characterization of the tunnel barrier when small, low-leakage tunnel junctions are made. The junctions with Pb-Bi counterelectrodes had large areas ($\cong$0.005 $cm^2$) so self-shielding prevented us from measuring the value of the Josephson current which was characteristic of the barrier.

### 3.3.5 Junctions with Nb-Sn Base and Nb Counterelectrodes

A single attempt has been made to fabricate $Nb_3Sn$/Al(oxidized)/Nb tunnel junctions. Each layer was highly textured. The I-V curve in Figure 3.9 shows the high leakage currents we have observed in these junctions. Reference junctions with $Nb_3Sn$ base electrodes and Pb-Bi counterelectrodes as described in Section 3.3.2, again gave us confidence that high subgap currents were due to the same cause as in the junctions with Nb base electrodes discussed in Section 3.3.4. Consequently, the investigation of the problem can be done using either base material.

### 3.3.6 Concluding Remarks on Reference Junctions

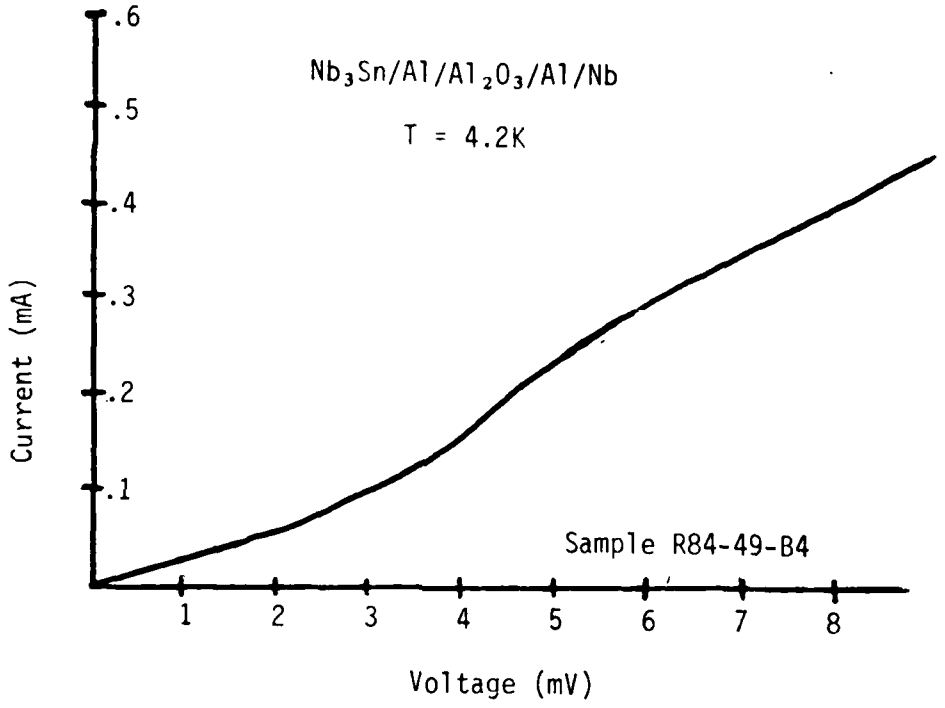


**Figure 3.9 The I-V characteristic of a Nb-Sn junction with a Nb counterelectrode.**

A summary of the various configurations of reference junctions is presented in Table 3.2. The role of barrier crystallinity was described for each type of junction in a qualitative fashion in Sections 3.3.1 to 3.3.5. A quantitative indicator of the subgap conductance which is included in Table 3.2 is the ratio of the current above the gap to the current below the gap measured at 4.2K. We have used I(4 mV)/I(2 mV) for junctions with a sum of gaps less than 4 mV, and I(6 mV)/I(3 mV) for junctions with a sum of gaps greater than 4 mV ($Nb_3Sn$-based junctions). The values of the current ratios are consistent with the qualitative discussion.

Another indicator of junction quality, $V_m$, is the product of the resistance measured at 2 mV (3 mV for high-gap materials) and the Josephson current. Measurements of the Josephson currents were not made for our large-area junctions because self-shielding would give low values uncharacteristic of intrinsic barrier properties. An estimate of $V_m$ can be made from theoretical estimates of the $i_cR_n$ product, the product of the Josephson current and the normal state tunneling resistance. Following Gurvitch, $V_{m(est)}$ would have a value in millivolts on the order of 1/2 to 1 times the ratio, I(4 mV)/I(2 mV), depending on the thickness of a proximity layer on either side of the barrier.[18]

A comparison must be made between the values of I(4 mV)/I(2 mV) in Table 3.2 and the current state of the art. Nb-based junctions made at IBM with an rf plasma oxidized native oxide barrier and a Pb-In-Au counterelectrode had $V_m$ = 28 mV and I(4 mV)/I(2 mV) = 30.[19] Gurvitch and co-workers have not published any data measured at 4.2K on junctions with soft-alloy coun-

| Junction Configuration | Barrier Crystallinity | I(4 mV)/ I(2 mV) |
|---|---|---|
| sp Nb / sp ox Al / Pb-Bi | polycrystalline | 30 - 60 |
| ev Nb / sp ox Al / Pb-Bi | highly-textured | 30 |
| ev Nb / ev ox Al / Pb-Bi | highly-textured | 2 - 5 |
| ev Nb / ev ox Al / Pb-Bi | Ion-milled, amorphous | 15 |
| ev Nb / ev ox Y / Pb-Bi | highly-textured | 2 - 4 |
| ev Mo-Re/sp ox Al / Pb-Bi | polycrystalline | 60 |
| sp Mo-Re/sp ox Al / Pb-Bi | polycrystalline | 20 |
| ev Nb-Sn/ev ox Al / Pb-Bi | highly-textured | 30 - 80 |
| ev Nb-Sn/ ev ox Y / Pb-Bi | highly-textured | 45 |
| ev Nb/ev ox Al/ ev Al/ Nb | all-epitaxial | 2 - 5 |
| ev Nb/sp ox Al/ sp Al/ Nb | highly-textured | 2 - 5 |
| evNb-Sn/ev ox Al/ev Al/Nb | highly-textured | 2 - 4 |

Table 3.2 - A comparison of the tunneling current at 4.2K above and below the sum of the gap voltages (I(4 mV)/I(2 mV) for Nb-based junctions and I(6 mV)/ I(3 mV) for Nb-Sn junctions) with the barrier structure of each type of junction. sp - sputtered ev - evaporated ox - oxidized

terelectrodes, but have reported all-Nb junctions with oxidized Al barriers with $V_m$ = 48 mV and I(4 mV)/I(2 mV) = 48 at 4.2K.[18] The best tunnel junctions with a $Nb_3Sn$ base were prepared by Rudman using an amorphous silicon barrier.[13] The ratio, I(4 mV)/I(2 mV) = 40 for data which was recorded at 1.4K.

Results obtained for reference junctions with Nb, $Nb_3Sn$, and Mo-Re base and counterelectrodes permitted us to to attain the first and third goals of those listed in the introduction to Section 3.3, and also to advance the second. Most importantly, we attained state-of-the-art, low-leakage I-V tunnelling characteristics for high-$T_c$ base electrodes with oxidized aluminum and yttrium overlayers. Thus we have reproduced and extended the recent results of Geerk et al.[14] We have also observed, for the first time, a definite dependence of the subgap leakage current upon the texture of the metal overlayer and oxide, and the deposition method. A systematic study of this important dependence is, unfortunately, beyond the scope of this program.

High leakage currents observed to date in all-Nb or $Nb_3Sn$ base/Nb counterelectrode tunnel junctions with $Al/Al_2O_3/Al$ barrier structures present a problem that we have not yet solved but have formulated an approach to solving. Since nearly ideal I-V characteristics have been attained in two other laboratories for all-Nb junctions with $Al/Al_2O_3/Al$ barriers, it is clear that a solution to the problem exists. It is also highly probable that the high leakage is related to the barrier crystallinity (extent of texture), or some unidentified effect related to the interface between aluminum oxide and the protective Al overlayer, or both. Current work is concentrating on this problem. Once a solution is

found, we will be in position to use the Nb counterelectrode as a reference for the investigation of high-$T_c$ counterelectrode homogeneity and crystalline order by tunnelling, i.e. within a distance from the barrier less than the coherence length (about 50 A for $Nb_3Sn$). The fourth goal of this task will, therefore, be attained.

Additional reference bilayer junctions with high-$T_c$ base electrodes will have to be deposited and processed at elevated temperatures to fully attain the second goal. and thus determine the highest temperature permissible for high-$T_c$ counterelectrode fabrication.

## 3.4 Task 4 - High-Transition Temperature Counterelectrode Fabrication

In the case of Mo-Re, a preferred approach to high-$T_c$ counterelectrode fabrication has been advanced. Mo-Re films have been sputtered and evaporated at a range of substrate temperatures from 100 to 800°C to see if the substrate temperature during counterelectrode formation could be held low enough to prevent interdiffusion of atoms in the barrier and superconductor. Films evaporated at 100°C in a background pressure of $<10^{-10}$ torr had the same $T_c$, room temperature resistivity, and resistivity ratio as those deposited at 800°C. The only observed difference was that RHEED patterns from the 100°C deposit did not indicate any texturing whereas the films grown at high temperature were highly textured.

The $T_c$ values for the films grown at 100°C are plotted versus composition determined by EDS in Figure 3.10 along with $T_c$

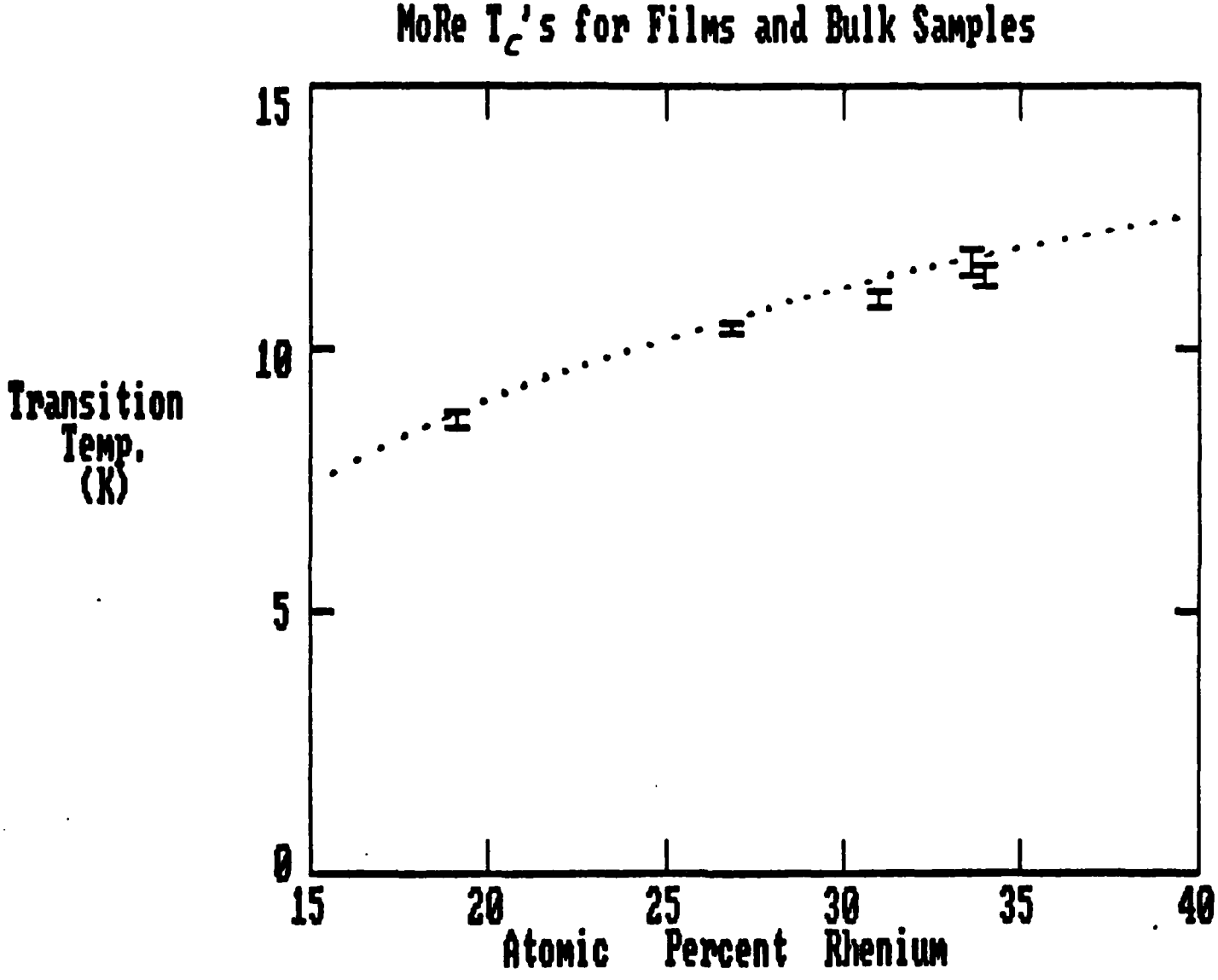


Figure 3.10 Resistive transition temperature plotted as a function of composition for MoRe alloys. The dotted line is a fit to data from the bulk samples of reference 15.

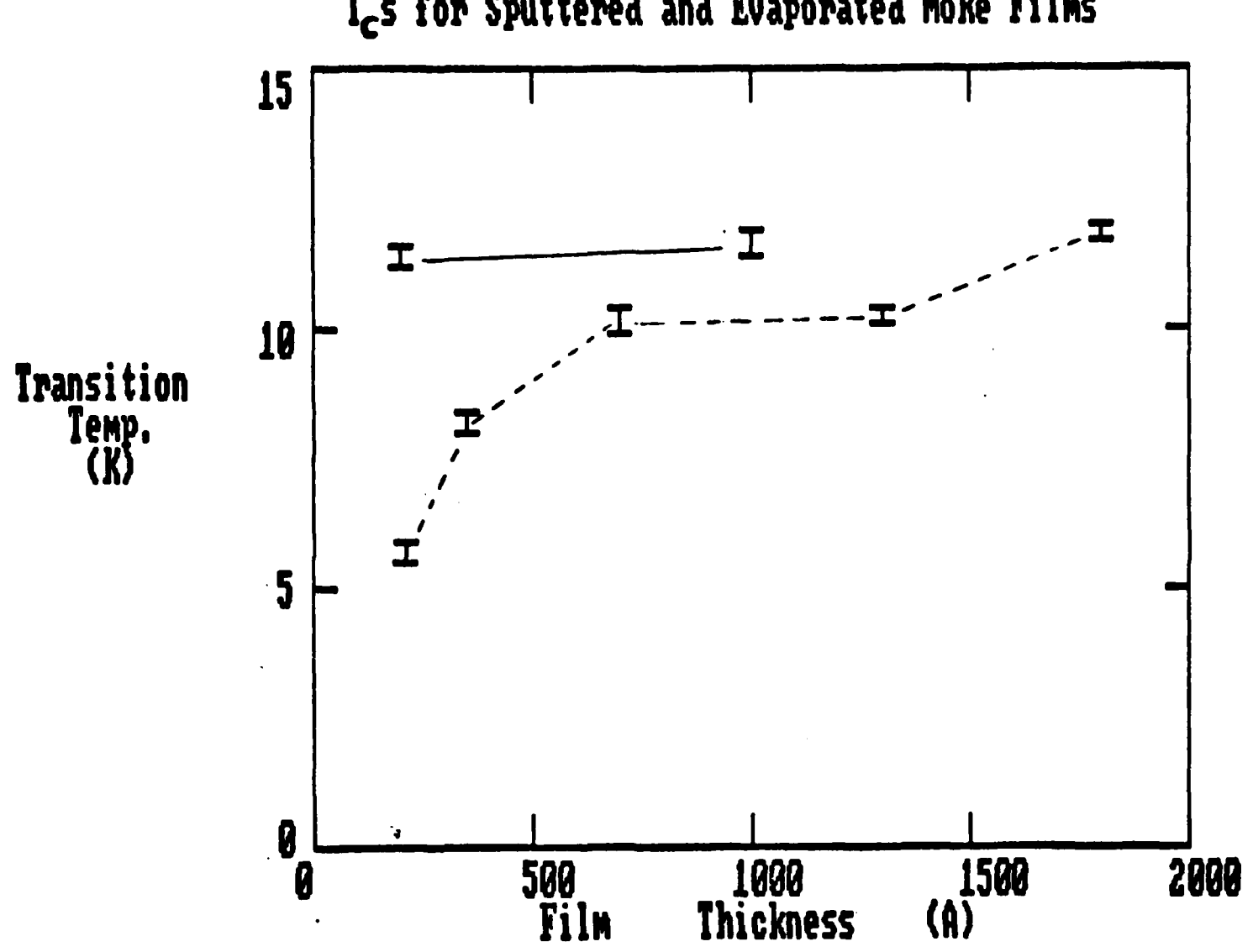


Figure 3.11 Resistive transition temperature for $Mo_{65}Re_{35}$ alloys plotted as a function of film thickness. The data for the films evaporated on substrates held at 100°C are connected by a solid line. The data for films sputtered at 800°C are connected by a dashed line.

data for bulk samples from Blaugher et al.[15] There has been no indication that any higher-$T_c$ phase other than the bcc alloy has formed. The A15 phase reported by Gavaler had a higher $T_c$ than the bulk samples (up to 15K) over the entire range of compositions shown in Figure 3.10.[16]

Films with the composition $Mo_{65}Re_{35}$ have been grown to thicknesses from 200 A to 1 μm. The $T_c$ of evaporated films, plotted in Figure 3.11, showed little change as a function of film thickness even though the substrate temperature was only 100°C. The resistivity ratios of the same samples, plotted as a function of film thickness in Figure 3.12, showed that there was no increase in disorder or in the incorporation of impurities in the thin evaporated film. The sputtered films, shown for comparison, had a sharp reduction in $T_c$ below a thickness of 1000 A along with a decrease in the resistivity ratio despite being deposited at 800°C. The sputtering was done in a small diffusion-pumped chamber with a background pressure of $10^6$ torr. We have attributed the $T_c$ and resistivity properties to the high level of impurities incorporated into the film during sputtering.

$Mo_{65}Re_{35}$ evaporated in a true UHV background appears to have all the characteristics needed for a 12K counterelectrode which can be formed at 100°C. No experiments have been performed in the SDAF on the low temperature growth of a higher-$T_c$ counterelectrode candidate. However, the RHEED pattern shown in Figure 3.13a of a 60 A thick film of $Nb_3Sn$ deposited at 900°C was an indication that the initial layer of material had nearly the same degree of crystalline order as a thick film. Figure 3.13b shows the RHEED pattern of the same sample later in the deposi-

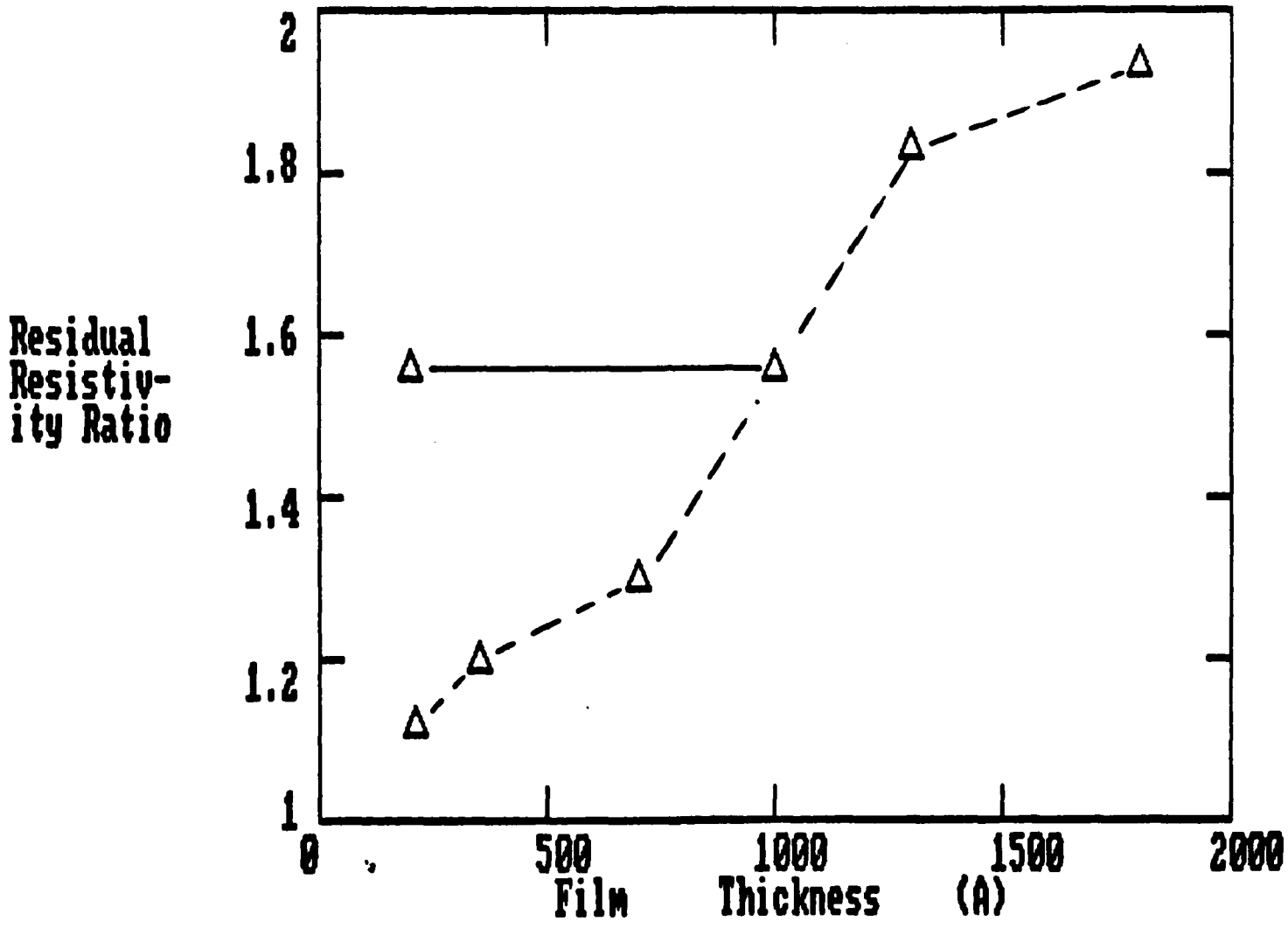


Figure 3.12 The resistivity ratio of $Mo_{.65}Re_{.35}$ alloys plotted as a function of film thickness. The data for the evaporated films are connected by a solid line. The data for films sputtered at 800°C are connected by a dashed line.

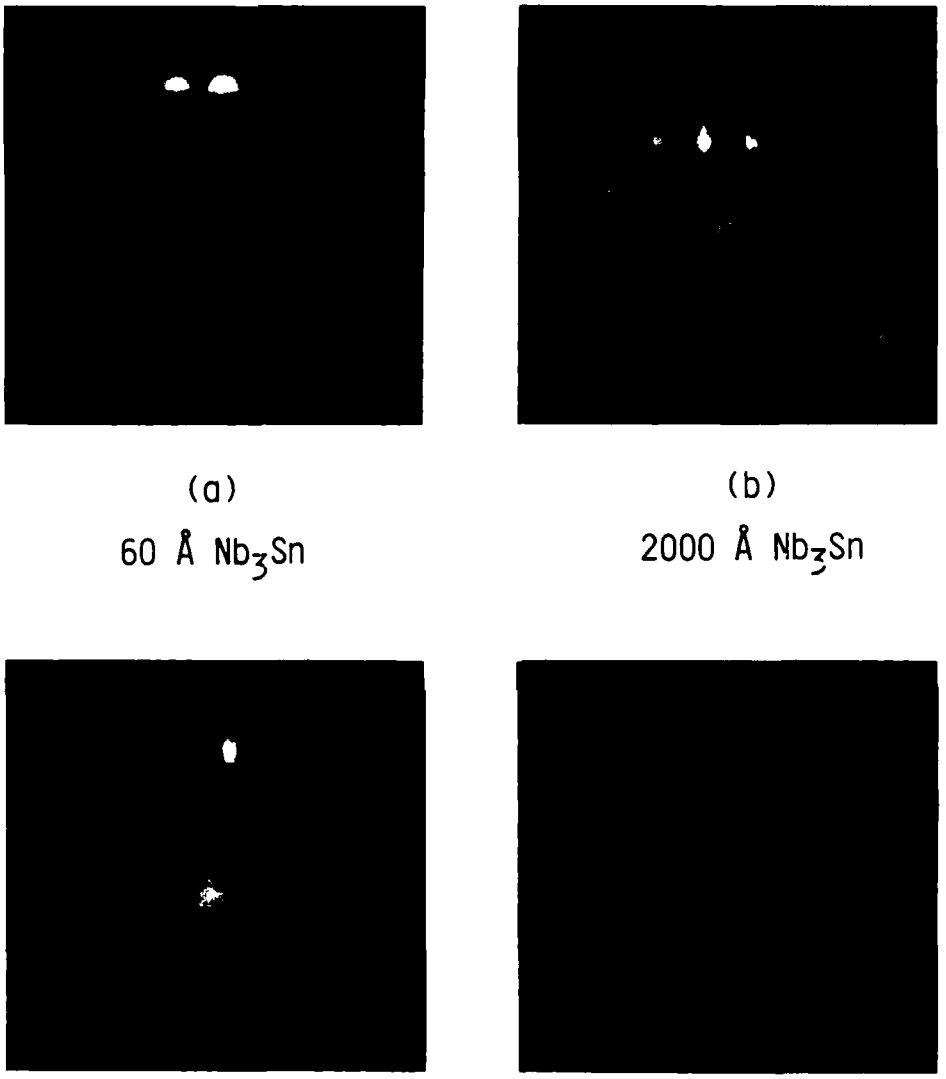

(a)
60 Å $Nb_3Sn$

(b)
2000 Å $Nb_3Sn$

(c)
Highly textured
30 A thick Al barrier

(d)
Polycrystalline
Al barrier

**Figure 3.13 RHEED patterns for four films.**

tion. The highly-textured structure was the same as after 60 A was grown although the spots were a bit sharper for the thick film.

Figure 3.13c is the RHEED pattern of the Al overlayer grown by evaporation on the $Nb_3Sn$ surface used for Figure 3.13b. Figure 3.13d is shown to contrast the RHEED pattern of a randomly-oriented polycrystalline overlayer with the highly-textured overlayer of Figure 3.13c. Experiments with epitaxial growth conducted as part of the cost-shared Westinghouse-AFOSR program using Nb/Al bilayers have shown that a thin (<40 A) overlayer of Al deposited on the oxidized surface of a bilayer can have the same texture as the first Al overlayer. The second Nb layer deposited as a counterelectrode had the same highly-textured RHEED pattern as the base Nb layer.

There have not been any attempts to grow A15 counterelectrodes. Several preliminary steps will have to be taken first:

1. The high subgap leakage current (Sections 3.3.4 to 3.3.6) tentatively ascribed to the $Al/Al_2O_3$ interface states must be significantly reduced.

2. XPS measurements of the behavior of the tunnelling barrier at high temperatures, of the type discussed in Sections 3.1 and 3.3.6, will have to be completed to establish a maximum processing temperature.

3. Thin (200 A) films of $Nb_3Sn$ will be deposited at high temperature to see if the crystalline order which has already been observed in the initial deposit will give rise to a high

$T_c$. The temperature of deposition will depend on the maximum temperature the barrier can withstand.

4. An alternative to high-temperature deposition is to deposit the counterelectrode material at room temperature and anneal the entire trilayer. Several 200 A $Nb_3Sn$ films have been deposited on sapphire and on 50 A of yttrium at room temperature and annealed for 1 hour at 700 and 800°C. The $T_c$ values were 13 and 14K for the two annealing temperatures and were independent of the underlayer material. A comparison must be made between this method and high-temperature deposition.

3.5 Task 5 - Fabricate and Test High-Operating Temperature Junctions

Although this task was not anticipated in the proposal to be started until the last six months of the project, attempts to form junctions with $Nb_3Sn$ base and Mo-Re counterelectrodes can be made in light of the success of that part of Task 4 which dealt with Mo-Re. One parameter which has not been varied to date is the thickness of the layer of normal metal deposited between the barrier and counterelectrode. We have only followed Gurvitch who has found that for polycrystalline $Al_2O_3$ barriers and Nb counterelectrodes, a 20-40 A layer of Al protected the Nb from reacting with oxygen adsorbed on the surface of the $Al_2O_3$ and consequently increased $V_m$ by a factor of two.[17]

In parallel with a systematic investigation of the leakage effects in the $Al_2O_3$/Al/Nb structure, we plan to vary the thickness of the protective Al layer (from 0 to 100 A) while using Mo-Re counterelectrodes, and replace Al with another material. We

believe that this approach will soon result in $Nb_3Sn$/Mo-Re high-$T_{op}$ tunnel junctions.

## 4. CONCLUSIONS

1. The investigation under Task 1 has determined the deleterious effect of the surface atomic segregation in high-$T_c$ A15 base electrodes, particularly for $V_3Si$. We have replaced $V_3Si$ with $Nb_3Sn$ as the base electrode on which we will focus our efforts.

2. The investigation under Task 2 resulted in a convenient and reliable process capable of patterning all-refractory A15, Mo-Re, and Nb test junctions.

3. The investigation under Task 3 resulted in:

   (a) high-$T_c$/soft counterelectrode tunnel junctions with excellent I-V characteristics.

   (b) discovery of the dependence of subgap leakage current on the barrier crystallinity (extent of texture).

   (c) definition of a problem, so far specific to Nb counterelectrodes, causing high leakage. We have tentatively attributed the problem to the interface between a highly textured oxide barrier and a thin metallic Al protective overlayer.

4. The investigation under Task 4 confirmed that Mo-Re is an ideal candidate for counterelectrodes with a $T_c$ of 12K.

## 5. ACKNOWLEDGEMENTS

The authors would like to acknowledge the assistance of P. D. Vecchio with fabrication of tunnel junctions from trilayers, R. Wilmer with Mo-Re depositions, K. Goodwill with sputtering $V_3Si$, A. L. Foley with modifications made to the SDAF, and J. R. Gavaler with interpretation of some results. A. S. Manocha has been an advisor for XPS throughout the program.

## 6. REFERENCES


1. J. Talvacchio, A. I. Braginski, J. R. Gavaler, M. A. Janocko, A. S. Manocha, and R. D. Blaugher, "Thin Film Technology of High-Critical-Temperature Superconducting Electronics," Annual Report, ONR Contract No. N00014-82-C-0617, December 5,1983

2. J. Kwo, G. D. Wertheim, M. Gurvitch, and D. N. E. Buchanan, "X-ray Photoelectron Study of Surface Oxidation of Nb/Al Overlayer Structures," Appl. Phys. Lett., 40(8), p675, 1982

3. M. Grundner, "On Oxide Thickness Measurements with ESCA," Proc. 7th Intl. Vac. Cong., p2237, Vienna, 1977

4. J. M. Graybeal and M. R. Beasley, "Localization and Interaction Effects in Ultrathin Amorphous Superconducting Films," Phys. Rev. B, 29, p4167, 1984

5. J. G. Simmons, "Low-Voltage Current-Voltage Relationship of Tunnel Junctions," J. Appl. Phys., 34, pp238-239, 1963

6. H. Ihara, Y. ▽imura, H. Okumura, K. Senzaki, and S. Gonda, "Oxidation Mechanism of the surface of A15 Superconductors," Adv. in Cryogenic Engineering, Vol. 30 - Materials, pp. 589-600, 1984

7. D. A. Rudman, R. E. Howard, D. F. Moore, R. B. Zubeck, and M. R. Beasley, "Fabrication and Barrier Diagnostics of Superconductive Tunnel Junctions of Nb-Sn and V-Si," IEEE Trans., MAG-15(1), pp148-150, January, 1979

8. E. L. Wolf, J. Zasadzinski, J. W. Osmun, and G. B. Arnold, "Proximity Electron Tunneling Spectroscopy I. Experiments on Nb," J. of Low Temp. Phys., Vol. 40(1,2), pp.19-50, 1980

9. H. Kroger, L. N. Smith, and D. W. Jillie, "Selective Niobium Anodization Process for Fabricating Josephson Tunnel Junctions," Appl. Phys. Lett., 39(3), p280, 1981

10. M. Gurvitch, M. A. Washington, H. A. Huggins, and J. M. Rowell, "Preparation and Properties of Niobium Josephson Junctions with Thin Aluminum Layers," IEEE Trans., MAG-19(3), p791, 1983

11. Handbook of Chemistry and Physics, 51 ed., 1971, pp D166-D172, CRC Press, Boca Raton, Florida,

12. M. Ronay and E. E. Latta, "Interaction of Nb Counterelectrodes with Aluminum Oxide and Rare-earth Oxide Tunnel Barriers," Phys. Rev. B, 27(3), p1605, 1983

13. D. A. Rudman, F. Hellman, R. H. Hammond, and M. R. Beasley, "A15 Nb-Sn Tunnel Junction Fabrication and Properties," J. Appl. Phys., 55(10), pp3544-3553, May,1984

14. J. Geerk (Nuclear Center, Karlsruhe), private communication, and U. Schneider, J. Geerk, and H. Reitschel, "Tunnel Spectroscopy on Superconducting $Nb_3Sn$ with Artificial Tunnel Barriers," Proc. LT-17, p489, 1984

15. R. D. Blaugher, A. Taylor, and J. K. Hulm, "The Superconductivity of Some Intermetallic Compounds," IBM J. of Res. and Dev., 6(1), p116, 1962

16. J. R. Gavaler, M. A. Janocko, and C. K. Jones, "A15 Structure Mo-Re Superconductor," Appl. Phys. Lett., 21(4), p179, 1972

17. M. Gurvitch, M. A. Washington, and H. A. Huggins, "High Quality Refractory Josephson Tunnel Junctions Utilizing Thin Al Layers," Appl. Phys. Lett., 42(5), p472, 1983

18. M. Gurvitch and J. Kwo, "Tunneling and Surface Properties of Oxidized Metal Overlayers on Nb," in Adv. in Cryogenic Engineering - Materials, Vol. 30, pp. 509-533, 1984

19. S. I. Raider and R. E. Drake, "Nb/Nb Oxide/Pb-alloy Josephson Tunnel Junctions," IEEE Trans., MAG-17(1), pp299-302, 1981

# TUNNELING AND INTERFACE STRUCTURE OF OXIDIZED METAL BARRIERS ON A15 SUPERCONDUCTORS

J. Talvacchio,* A. I. Braginski,* M. A. Janocko*
Westinghouse R&D Center, Pittsburgh, PA 15235

and S. J. Bending†
Hansen Laboratories, Stanford University, Stanford, CA 94305

## Abstract

A15-based tunnel junctions have been prepa ' with barriers of oxidized Al, Si, and Y. Properties of the superconductor/barrier interface which are crucial for low-leakage junctions were established by correlating XPS spectra of oxidized bilayers and RHEED patterns of the surface of each layer with tunneling characteristics. Comparisons were made between oxidized Al barrier properties for Nb and $Nb_3Sn$ base electrodes. Some differences between evaporated and dc magnetron sputtered barriers have emerged.

## Introduction

Recent work by Gurvitch and Kwo has correlated the physical properties of oxidized metal overlayers on Nb with electrical properties of the overlayers used as tunneling barriers.[1] Our objective has been to extend that type of study to A15-based tunnel junctions. Our choice of Al and Y as the focus of the study was based on Gurvitch and Kwo's evidence that Al and Y layers < 20 Å thick provide complete coverage of a Nb surface, and some requirements which are more important for A15-based junctions than for Nb. The use of high-$T_c$ superconductors as counterelectrodes will probably require high temperature processing. Both $Al_2O_3$ and $Y_2O_3$ are stable oxides at temperatures of interest (< 1000°C) without suboxides. Yttrium and the rare earth elements which have a similar chemistry were considered because the diffusion rates of such massive atoms are lower.

The crystallinity of the tunneling barrier may be more important for A15 junctions than for Nb because atomic order in the first 50 Å (about one coherence length) of an A15 counterelectrode is more critical than for Nb with its longer coherence length.

## Sample Preparation

Deposition of $Nb_3Sn$ and $V_3Si$ base electrodes was carried out in a multiple-chamber UHV system with facilities for deposition and in situ surface analysis. Sapphire substrates were clamped to a molybdenum block heated to 800 to 900°C as measured by a W-5% Re/W-26% Re thermocouple inserted in a cavity in the block. The molybdenum block was rotated at about 20 rpm in the case of evaporation or oscillated in front of the target at 20 cycles per minute in the case of dc magnetron sputtering. After the samples cooled to < 200°C, barrier layers of Al or Y were either sputtered or evaporated without removal from vacuum. Some variations in the oxidation procedure will be discussed but generally the samples were exposed to 100 millitorr of dry oxygen for an hour before removal from the system. They were kept in a controlled-humidity atmosphere (40%) during the 10 minutes required to paint on an insulating layer and load the samples for evaporation of a PbBi counterelectrode through an aperture mask.

The $V_3Ga$ films were evaporated by one of us (SJB) at Stanford with a similar procedure but using silicon barriers oxidized in air.

## Atomic Segregation at Oxidized A15 Surfaces

The native oxides of A15 superconductors usually form poor tunneling barriers.[2] Ihara et al. have shown qualitatively using X-ray Photoelectron Spectroscopy (XPS) that an atomic segregation of the constituents of an A15 compound occurred when the surface was oxidized.[3] Our data for $Nb_3Sn$, $V_3Si$, and $V_3Ga$ are shown in Table 1. The compositions listed in Table 1 which were derived from XPS measurements were based on elemental sensitivities compiled by the analyzer manufacturer modified by our own measurements of elemental standards.

The layer thicknesses were calculated using the integrated area of each photoelectron peak following Carlson and McGuire for the structure shown in Figure 1.[4] Their equations were based on the assumption that each layer had a uniform thickness and was on a flat substrate. A photoelectron escape depth of $\lambda$ = 20 Å was used for the tabulated data. The calculations have been repeated using $\lambda$ = 16 Å for metallic layers and $\lambda$ = 27 Å for oxide layers following Ermolieff et al. without any qualitative difference in the results.[5] Bulk densities were assumed in the calculation of layer thicknesses.

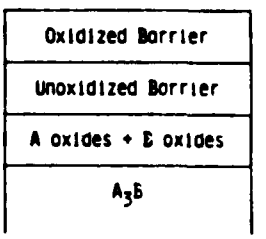


Figure 1 — The structure used to calculate layer thicknesses from XPS.

A greater limitation for our application of the Carlson and McGuire formulation was their restriction to photoelectron peaks with similar kinetic energies. Penn found that $V_2p$ photoelectrons with a kinetic energy of 742 eV (Mg $K\alpha$ X-rays) has $\lambda$ = 15 Å.[6] The other relevant photoelectrons have kinetic energies between 1000 eV and 1200 eV with $\lambda$ = 18 to 21 Å. If this difference was important, the lowest layer which contained V should have shown the greatest attenuation. However, the first row of Table 1 shows that the number of $V_2p$ photoelectrons detected even through a 100 Å barrier is sufficient to give a composition which agrees with the bulk composition from electron microprobe.

The entries in Table 1 for each A15 compound were ordered by increasing thickness of the oxidized A15 layer. The oxidation occurred either because there was

*Supported by ONR Contract No. N00014-82-C-0617.

*Supported in part by AFOSR Contract No. F49620-78-C-0031.

†Supported in part by DOE Contract No. DE-AT03-76ER71043 and ONR Contract No. N00014-83-K-0391.

Manuscript received September 10, 1984.

Table 1 – Surface Segregation of A15 Compounds

| Compound $A_3B$ | Sample # | Barrier Thickness (Å) | Oxidized A15 Thickness (Å) | Oxidized A15 % B Oxide | A15 Metal at. % B (XPS) | A15 Metal at. % B (bulk) |
|---|---|---|---|---|---|---|
| $V_3Si$ | 9-B5 | 100 | 0 | -- | 24 | 27 |
| | 3-B5 | 37 | 2 | 100 | 30 | 30 |
| | 4-B5 | 20 | 9 | 100 | 80 | 33 |
| | 8-B2 | 0 | 73 | 62 | 47 | 29 |
| | 8-B4 | 0 | > 100 | 72 | -- | 29 |
| $Nb_3Sn$ | 18-B5 | 50 | 0 | -- | 21 | 21 |
| | 33-B6 | 26 | 4 | 48 | 31 | 26 |
| | 13-B4 | 0 | 33 | 39 | 23 | 23 |
| $V_3Ga$ | 138-A10 | 20 | 0 | -- | 23 | 23 |
| | 114-A1 | 25 | 0 | -- | 22 | 21 |
| | 114-B1 | 25 | 11 | 45 | 22 | 29 |

no barrier or a very thin one, or in some cases because there was some exposure to oxygen before barrier deposition. The column which lists the percentage of B element oxide shows the extent of segregation which occurred during oxidation. It is the number density of B atoms in an oxide environment compared with the total number of A and B atoms which emit photoelectrons with a chemical shift characteristic of the oxide. By this definition, an $A_3B$ compound which was completely oxidized would have an entry of 25%.

When $V_3Si$ oxidized, $SiO_2$ formed first and a number of samples have also shown an increased silicon concentration in the metal underneath. There must have been a V-rich layer left behind which would be deep enough compared to the coherence length of 40 Å to affect tunneling properties. Sample 8-B4 had an oxide layer which was too thick to measure because it was dipped in water and left to dry in air.

The background pressure in the magnetron sputtering system where $V_3Si$ samples were made was typically $1 \times 10^{-8}$ torr with the pumping line throttled for introduction of argon. About 20 minutes were needed to return to this pressure after the base electrode was deposited. However, the sample block needed 30 minutes to cool to < 200°C and deposited films always showed 2 to 5 Å of surface oxide growth after that time. A liquid nitrogen-cooled quenching block was assembled which pressed against the edges of the sample block during the time between base electrode and barrier depositions to cut the cooling time to < 10 minutes. This procedure has led to an order of magnitude reduction in subgap currents. However, the $V_3Si$ transition temperatures have been less than 15K with correspondingly low gap values. We were limited to deposition rates (25 Å/min.) which were probably too low for a material which getters as well as vanadium.

The segregation of $Nb_3Sn$ was less dramatic than for $V_3Si$. $Nb_2O_5$ forms at the same time as $SnO_2$ but in a concentration less than 75%. In contrast to $V_3Si$, no change in the composition of the superconductor at the interface with its oxide was observed within the resolution of our measurements which is consistent with the fact that excellent tunnel junctions have sometimes been made with the native oxide of $Nb_3Sn$.[7] Nevertheless, we observed higher subgap currents in tunnel junctions with some base electrode oxidation due to exposure to humid air.

Figure 2 shows the current-voltage characteristic of an evaporated $Nb_3Sn$ junction with 20 Å of $Al_2O_3$, 12 Å of Al, and no base electrode oxides. The transition temperature of this particular sample was about 0.1K wide at 17.5K. However, the width of the gap, 0.6 mV, was typical of our junctions and those made by Rudman and co-workers.[8] The midpoint of the $Nb_3Sn$ gap, 3.25 meV, corresponded to $2\Delta/kT_c = 4.3$ which was also in agreement with data in reference 8. Although there was some leakage current even below the PbBi gap, the ratio of I(6 mV)/I(3 mV) = 60. Junctions which had similar XPS data had ratios from 35 to 80 which were comparable to Rudman's $Nb_3Sn$-based junctions with oxidized silicon barriers but with higher leakage below the PbBi gap and perhaps lower excess conductance below the sum of the gaps.[9]

Curve 747956-A

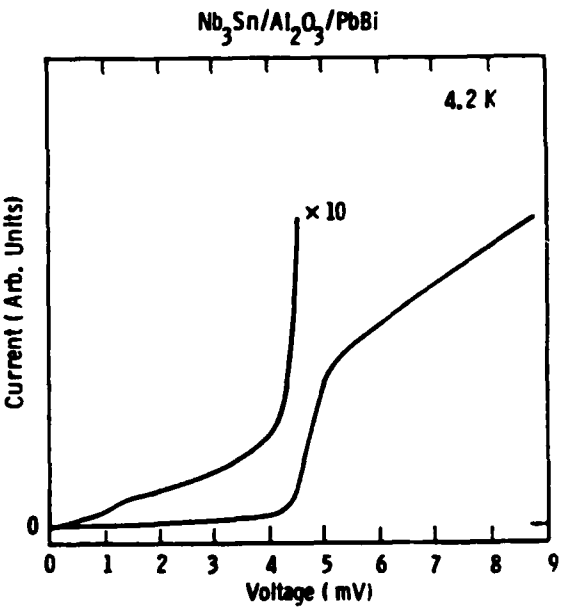


Figure 2 – Quasiparticle tunneling characteristic for a $Nb_3Sn$ junction with an oxidized, evaporated Al barrier and a PbBi counterelectrode.

In contrast to the samples which underwent a standard oxidation, identical bilayers which were left for several days in humid air before counterelectrode deposition had barriers with 25 Å of $Al_2O_3$ and 15 Å of a mixture of niobium and tin oxides. Values of I(6 mV)/I(3 mV) were 3 to 5. Despite having a thicker barrier, there was no increase in the junction resistance above the sum of the gaps, $R_n$. Therefore, the additional oxidation affected the electrical properties of the barrier as well as the surface of the $Nb_3Sn$.

The $V_3Ga$ samples had surface compositions similar to the bulk except for the sample with 11 Å of oxide growth. The oxide layer was deficient in vanadium oxide and the adjacent superconductor showed a small increase in Ga concentration. Junctions formed on samples 114-Al

and Bi had similar characteristics. However, the XPS measurements were made after the counterelectrode and insulator layers were stripped in acetic acid and acetone so oxidation of the $V_3Ga$ probably occured only after the junctions were measured. The tunneling data will be published separately.

The importance of avoiding the deleterious effects of A15 oxidation is analogous to the same need for Nb-based junctions. We observed a degradation of tunneling characteristics when Al barriers were too thin to protect underlying Nb base electrodes or when some oxidation occurred before the Al was deposited in agreement with a number of others such as Wolf.[10] However, the mechanism which leads to a weakly superconducting surface layer in several A15 materials is an atomic segregation rather than the suboxide formation that occurs at a niobium/niobium oxide interface.

## Tunneling Barrier Structure

XPS measurements have been useful but not sufficient indicators of junction quality. Some of our tunneling results have depended strongly on the crystallinity of the barrier which was a function of the base electrode structure and the deposition technique. Amorphous and crystalline oxide barriers have appeared to be identical by XPS analysis but consistently produced different tunneling results. Figure 3a is a Reflection High Energy Electron Diffraction (RHEED) pattern from the surface of 60 Å of $Nb_3Sn$ evaporated on epitaxial-grade sapphire of unknown orientation at 900°C. Figure 3b shows that the pattern did not change except that the spots became sharper after 2000 Å were deposited. The single orientation which we have tentatively identified as (111) indicated that the film was very highly textured even after just 60 Å were grown. The probable reason we obtained such well-ordered material was that the pressure during evaporation was $< 10^{-9}$ torr.

Thin overlayers of Al or Y which were deposited on such highly textured films of either Nb or $Nb_3Sn$ generally displayed RHEED patterns such as that shown in Figure 4a for a 30 Å thick Al layer deposited at 75°C on $Nb_3Sn$. The I-V curve in Figure 2 was from this type of structure. The RHEED pattern in Figure 4b was from a 40 Å polycrystalline Al layer deposited on a polycrystalline Nb base.

The type of RHEED patterns obtained and their relation to subgap tunneling currents for a number of base electrode/barrier configurations are summarized in Table 2. The ratio I(6 mV)/I(3 mV) is used as a measure of junction quality [I(4 mV)/I(2 mV) for Nb]. Patterns such as the one shown in Figure 4a are designated HT for highly textured. Polycrystalline patterns and patterns indicative of amorphous surface layers are labeled PC and AM, respectively. Overlayers formed on superconductors with HT surfaces had a diffraction pattern showing a single orientation but with spacings characteristic of the overlayer crystal structure. After oxidation there was still a single orientation but the pattern reflected the oxide's structure.

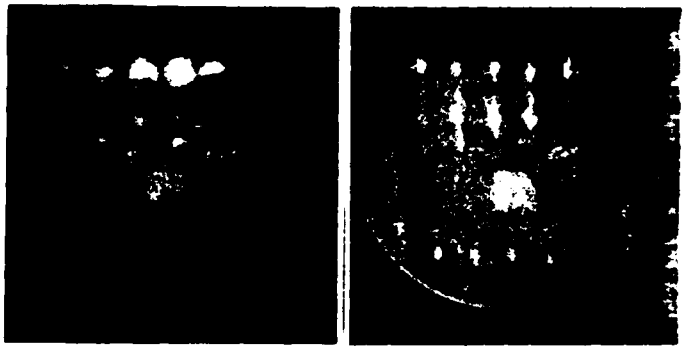

(a) 60 Å $Nb_3Sn$ (b) 2000 Å $Nb_3Sn$

Figure 3 – (a) RHEED pattern of the surface of a highly-textured 60 Å thick $Nb_3Sn$ film grown on epitaxial-grade sapphire. (b) RHEED pattern of the surface of the same film after 2000 Å were deposited.

Single-orientation Al barriers evaporated on Nb made poor tunneling barriers in a number of experiments although they worked well for $Nb_3Sn$ and appeared from XPS measurements to be identical to sputtered barriers. On the other hand, sputtered Al barriers have worked well on Nb regardless of their structure. The surface of one group of evaporated Nb/Al bilayers was bombarded after oxidation with 600 eV argon ions for 15 minutes at 0.5 $\mu A/cm^2$. The $Al_2O_3$ became amorphous and the subgap currents were lower. There was no change in the XPS spectra due to the ion milling. A similar treatment of yttrium oxide barriers has not yet been tried.

The last columns of Table 2 compare the oxide barrier thickness from XPS with parameters fitted to the quantum mechanical tunneling theory derived by Simmons.[11] The ratio of the current to the voltage should be linear in the voltage squared if the low-voltage limit of Simmons' model is used. The tunneling current was fitted to a two-term polynomial function of voltage up to 0.4V. The

Table 2 – Relation between RHEED Patterns and Junction Quality

| Base Material/ RHEED | Barrier before Oxidation/ RHEED | RHEED after Oxidation | I(6 mV)/ I(3 mV) | Oxide Thickness (Å) | | Barrier Height, $\bar{\phi}$ (eV) |
|---|---|---|---|---|---|---|
| | | | | XPS | S(Simmons) | |
| ev. $Nb_3Sn$/HT | ev. Al/HT | HT | 30 to 80 | 20 | 16 | 1.4 |
| | sp. Al/HT | HT | --* | 20 | -- | -- |
| ev. Nb/HT | ev. Al/HT | HT | 2 to 5 | 18 | -- | -- |
| | ev. Al/HT | AM* | 15 | 18 | 27 | 1.0 |
| | ev. Y/HT | HT | 2 to 4 | 43 | 16 | 1.9 |
| | sp. Al/HT | HT | 30 | 18 | 14 | 2.4 |
| sp. Nb/PC | sp. Al/PC | -- | 30 to 60 | 18 | 14 | 2.0 |

*$Nb_6Sn_5$ phase present in these samples.

*Ion-milled after oxidation.

barrier height, $\bar{\phi}$, and barrier width, S, were calculated from the fitting parameters following Simmons. An indication of how well a rectangular barrier simulated real barriers is given in Figure 5 for a highly textured Al barrier on $Nb_3Sn$ where a plot of I/V versus $V^2$ is shown to be a reasonably straight line. At voltages greater than 0.4V where the low-voltage limit no longer applies, the current rises faster than $V^3$. An asymmetry about zero bias was observed for all samples but was small enough that it will not be discussed here. Rowell found S = 14 Å and $\bar{\phi}$ = 1.95 eV for $Al_2O_3$ barriers on Al.[12] Our samples had a range of barrier heights with values which were significantly higher for sputtered barriers than for evaporated barriers.

(a) Highly textured 30 A thick Al barrier

(b) Polycrystalline Al barrier

Figure 4 – (a) RHEED pattern of a highly-textured Al film 30 Å thick evaporated on $Nb_3Sn$. (b) RHEED pattern of a polycrystalline Al overlayer 40 Å thick with no preferred orientation.

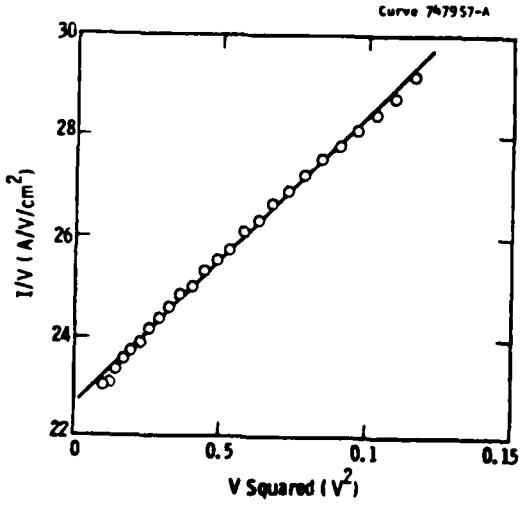


Figure 5 – I/V versus $V^2$ for a $Nb_3Sn$ junction with an oxidized, evaporated Al barrier fitted by a straight line following Simmons' low-voltage limit for tunneling through a rectangular barrier.

For Al, the barrier widths from Simmons' model were slightly smaller than those measured by XPS. XPS measurements of barrier thickness taken with the detector at glancing angles to the sample surface indicated that the barriers may not have been of uniform thickness, particularly for sputtered overlayers.[13] Although the Simmons' model should have reflected the thinner parts of the barrier and the XPS data measured an average thickness, the differences were too small to confirm the glancing angle XPS. The samples with evaporated $Al_2O_3$ barriers which were milled with an ion beam to make them amorphous had a broad (27 Å), low (1.0 eV) barrier. Ruggiero and co-workers suggested that such a barrier shape indicates the presence of a degraded base electrode surface layer.[14] The samples with amorphous barriers had higher leakages than those with sputtered barriers but had no decrease in the size of the gap. The barrier width calculated for evaporated Y should be considered as a lower limit of the value which might be obtained for a low-leakage junction.

## Conclusions

1. Atomic segregation of the components of A15 compounds upon oxidation causes a degradation of A15-based tunnel junctions.

2. Evaporated, highly textured Al overlayers produce low-leakage barriers on A15 $Nb_3Sn$. In contrast, Al evaporated on Nb results in high leakage currents.

3. Barriers formed by oxidation of Al evaporated on $Nb_3Sn$ exhibit a barrier height lower than those of Al sputtered on Nb.

4. The crystallinity of Al sputtered on Nb does not affect the leakage current.

5. Although neither is sufficient by itself, XPS and RHEED indicate the quality of artificial tunneling barriers during fabrication on A15 base electrodes.

## Acknowledgements

The authors want to acknowledge the assistance of K. Goodwill with $V_3Si$ depositions and Mrs. M. B. Cross with preparation of this manuscript.

## References

1. M. Gurvitch and J. Kwo, in Adv. in Cry. Eng. – Mat., 30, p. 509, 1984.
2. D. A. Rudman and M. R. Beasley, Appl. Phys. Lett., 36(12), p. 1010, 1980.
3. H. Ihara, Y. Kimura, H. Okumura, K. Senzaki, and S. Gonda, Adv. in Cry. Eng. – Mat., 30, p. 589, 1984.
4. T. A. Carlson and G. E. McGuire, J. Elec. Spec. and Related Phen., 1, p. 161, 1972.
5. A. Ermolieff, M. Girard, C. Raoul, C. Bertrand, and T. Minh-duc, presented at the 6th Symp. on Appl. Surface Anal., Dayton, Ohio, 1984.
6. D. R. Penn, Elec. Spec. and Related Phen., 9(1), p. 29, 1976.
7. D. A. Rudman, R. E. Howard, D. F. Moore, R. B. Zubeck, and M. R. Beasley, IEEE Trans., MAG-15(1), p. 148, 1979.
8. D. A. Rudman, F. Hellman, R. H. Hammond, and M. R. Beasley, J. Appl. Phys., 55(10), p. 3544, 1984.
9. D. A. Rudman, Ph.D. Thesis, Stanford Univ., 1982.
10. E. L. Wolf, J. Zasadzinski, J. W. Osmun, and G. B. Arnold, J. of Low Temp. Phys., Vol. 40(1,2), p. 19, 1980.
11. J. G. Simmons, J. Appl. Phys., 34, p. 238, 1963.
12. J. M. Rowell in Tunneling Phenomena in Solids, ed. E. Burstein and S. Lundqvist, Plenum Press, New York, 1969.
13. J. Talvacchio, A. I. Braginski, and M. A. Janocko, presented at March Mtg. of the APS, Detroit, 1984.
14. S. T. Ruggiero, G. B. Arnold, E. Track, and D. E. Prober, Proc. 17th Intl. Conf. on Low Temp. Phys., North-Holland, Amsterdam, 1984.

END

FILMED

3-85

DTIC